Article

Cell Reports

Gamma Oscillations in Rat Hippocampal Subregions Dentate Gyrus, CA3, CA1, and Subiculum Underlie Associative Memory Encoding

Graphical Abstract

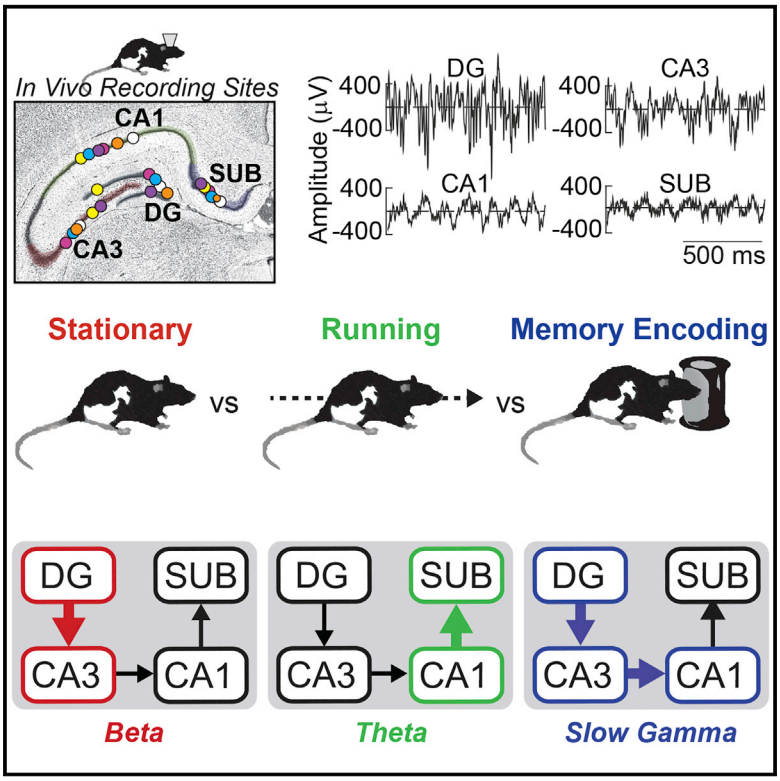

Highlights

- Slow gamma activity characterized hippocampal LFPs when rats explored objects
- Slow gamma increase could not be explained by cessation of locomotion
- Slow gamma during familiar object exploration correlated with novelty
- Slow gamma during novel object exploration related to subsequent associative memory

Authors

John B. Trimper, Claire R. Galloway, Andrew C. Jones, Kaavya Mandi, Joseph R. Manns

Correspondence

jmanns@emory.edu

In Brief

Hippocampal local field potentials are modulated by both memory and behavior. Trimper et al. describe how these factors interact to influence the hippocampal network state and demonstrate that slow gamma activity in particular correlates with associative memory encoding.

Trimper et al., 2017, Cell Reports *21*, 2419–2432
November 28, 2017 © 2017 The Author(s).
https://doi.org/10.1016/j.celrep.2017.10.123

Cell Reports
Article

OPEN ACCESS
CellPress

Gamma Oscillations in Rat Hippocampal Subregions Dentate Gyrus, CA3, CA1, and Subiculum Underlie Associative Memory Encoding

John B. Trimper,[1] Claire R. Galloway,[1] Andrew C. Jones,[2] Kaavya Mandi,[2] and Joseph R. Manns[1,3,*]
[1]Department of Psychology, Emory University, Atlanta, GA 30322, USA
[2]Neuroscience and Behavioral Biology Program, Emory University, Atlanta, GA 30322, USA
[3]Lead Contact
*Correspondence: jmanns@emory.edu
https://doi.org/10.1016/j.celrep.2017.10.123

SUMMARY

Neuronal oscillations in the rat hippocampus relate to both memory and locomotion, raising the question of how these cognitive and behavioral correlates interact to determine the oscillatory network state of this region. Here, rats freely locomoted while performing an object-location task designed to test hippocampus-dependent spatial associative memory. Rhythmic activity in theta, beta, slow gamma, and fast gamma frequency ranges were observed in both action potentials and local field potentials (LFPs) across four main hippocampal subregions. Several patterns of LFP oscillations corresponded to overt behavior (e.g., increased dentate gyrus-CA3 beta coherence during stationary moments and CA1-subiculum theta coherence during locomotion). In comparison, slow gamma (~40 Hz) oscillations throughout the hippocampus related most specifically to object-location associative memory encoding rather than overt behavior. The results help to untangle how hippocampal oscillations relate to both memory and motion and single out slow gamma oscillations as a distinguishing correlate of spatial associative memory.

INTRODUCTION

Neuronal oscillations reflect rhythmic fluctuations of transmembrane ion currents summed across neurons (Buzsáki et al., 2012). This rhythmicity modulates the timing—and thus the efficacy—of synaptic transmission and synaptic plasticity (Huerta and Lisman, 1995; Hyman et al., 2003; Orr et al., 2001; Zarnadze et al., 2016), shaping interactions between populations of neurons within and across brain regions (Engel et al., 2001; Fries, 2015; Singer, 1999; Varela et al., 2001). Depending on the brain region, oscillatory activity often correlates with overt behaviors, such as reaching or locomotion (Ahmed and Mehta, 2012; MacKay and Mendonça, 1995), or with covert cognition, such as attention (Tiitinen et al., 1993; Tallon-Baudry et al., 1997; Fries et al., 2001; Jensen et al., 2007) or memory (Igarashi et al., 2014; Montgomery and Buzsáki, 2007; Jutras et al., 2009, 2013; Shirvalkar et al., 2010; Trimper et al., 2014). Much progress has been made in understanding how neuronal oscillations in sensory (Brovelli et al., 2004; Nicolelis et al., 1995), motor (Engel and Fries, 2010; MacKay and Mendonça, 1995), and cognitive (Herrmann et al., 2004; Colgin, 2016) systems relate to the respective functions of these systems by mediating well-timed interactions within and across neuronal networks. A major remaining challenge is to understand how multiple neuronal oscillations with differing cognitive and behavioral correlates can interact to determine the oscillatory network state of a brain region.

One brain region exhibiting oscillatory activity correlated with both cognition and overt behavior is the hippocampus. In particular, neuronal oscillations in the hippocampus relate closely to both memory and movement (Colgin, 2016, for review). For example, in the rodent hippocampus, local field potential (LFP) oscillations in the theta (6–10 Hz), slow gamma (30–55 Hz), and fast gamma (65–90 Hz) frequency ranges relate not only to memory performance but also to running speed outside of explicit memory tasks (Kemere et al., 2013; Sławińska and Kasicki, 1998; Trimper et al., 2014; Winson, 1978; Zheng et al., 2016). Despite our good understanding of the relationship between hippocampal oscillations and locomotion, other important behaviors are underexplored. In semi-naturalistic settings, rats explore their environment in sporadic bursts of running, punctuated by frequent stops during which they often explore their surroundings, including the objects they would ordinarily encounter in real-world settings (Golani et al., 1993; Renner and Seltzer, 1991; Whishaw et al., 2006). However, little is known about the patterns of hippocampal oscillations during these moments of spontaneous exploration. This gap in knowledge about hippocampal oscillations during object exploration contrasts with the increasing use of spontaneous object recognition memory tasks in rodent studies (Clark and Squire, 2010) and with the widely held view of the mammalian hippocampus as being central to associating nonspatial items, such as objects, with spatial information, such as locations (e.g., Davachi, 2006; Knierim et al., 2006; Manns and Eichenbaum, 2006; Witter et al., 2000). Thus, an important question is how the patterns of oscillations in the hippocampus distinguish object exploration from other behaviors during spatial navigation and whether these oscillatory patterns relate to encoding object-location associative memories or more narrowly reflect the act of exploration.

This is an open access article under the CC BY license (http://creativecommons.org/licenses/by/4.0/).

To address this broad question, we recorded neuronal activity from the hippocampus as rats were tested for object-location associative memory while freely locomoting on a circular track. The specific questions were (1) whether patterns of hippocampal oscillations during exploration of objects would reflect more than the cessation of locomotion, and if so, (2) the extent to which these oscillations would correspond to memory for the object encounters rather than simply reflecting the act of exploration. We recorded spiking and LFPs from the principal cell layers of four major subregions of the hippocampus: dentate gyrus (DG), CA3, CA1, and subiculum. The goal in recording from all four regions simultaneously was to measure the functional dynamics of the local circuitry and assess potential heterogeneity across regions in terms of correlates with cognition and behavior. For example, by one view, dentate gyrus and CA3 are hypothesized to be particularly important for associative memory encoding, whereas CA1 and subiculum may be of greater importance for resolving discrepancies between internal and external representations in service of environmental navigation (Kesner and Rolls, 2015).

The results showed that the pattern of oscillatory activity across these four subregions clearly distinguished overt behaviors, differing prominently among moments of object exploration, stationary moments, and periods of locomotion. Moreover, when the pattern of oscillatory activity was contrasted across memory conditions during the single behavioral state of object exploration, slow gamma power and region-region coherence distinguished between exploring novel, repeated, and repositioned objects and, during exploration of novel objects, related to whether the rat would subsequently show good object-location associative memory. The results highlight the intersection of memory and locomotion in determining the oscillatory network state of the hippocampus and offer insights as to how oscillatory signatures of both behavior and cognition interact within a single brain region. The results also reveal that slow gamma oscillations across the major hippocampal subregions mark an oscillatory network state of effective associative memory encoding.

RESULTS

To ask how hippocampal network activity related to both memory and overt behavior, action potentials and LFPs were recorded simultaneously from DG, CA3, CA1, and subiculum in six rats as the animals performed a novel object recognition memory task that probed the rats' memory for objects and objects' locations. Figure 1 shows LFP recording sites in each of the four subregions in six rats, as well as example LFPs recorded from each of these four subregions during the approach and exploration of novel objects. The intra-hippocampal connectivity among DG, CA3, CA1, and subiculum is serial (Amaral and Witter, 1989); thus, a key initial question was how the oscillatory amplitude and synchrony between LFPs of connected subregions changed as rats engaged in object exploration behavior. Accordingly, Figure 1 also shows power and coherence during object approach and exploration (mean number of object encounters ± SEM across rats = 50.8 ± 8.6 events) across a range of frequencies between LFPs from connected regions (DG-CA3, CA3-CA1, and CA1-subiculum). Large increases in slow gamma coherence between DG and CA3 and between CA3 and CA1 were apparent during novel object exploration. Increases in slow gamma power during object exploration relative to the pre-exploration approach period were also visible in these regions. A main question of the present study was the extent to which this pattern of intra-hippocampal oscillatory synchrony reflected memory for the object encounters or simply the act of object exploration. However, because hippocampal activity was well known to be modulated by voluntary locomotion (Whishaw and Vanderwolf, 1973), a preliminary question was whether the pattern of oscillatory interactions observed reflected object exploration or just the cessation of locomotion.

Novel Object Exploration Elicited a Distinct Hippocampal Oscillatory State

As shown in Figure S1 for DG, CA3, CA1, and subiculum (and in previous reports for subsets of these subregions, e.g., Ahmed and Mehta, 2012; Kemere et al., 2013; Zheng et al., 2015), the frequency and amplitude of hippocampal LFPs—in theta, slow gamma, and fast gamma ranges—were strongly influenced by rats' speed of locomotion. Slow gamma power was at its relative highest across movement speeds in DG, CA3, and CA1 when rats were stationary. Thus, a possible explanation for the slow gamma coherence increase observed between DG and CA3 and between CA3 and CA1 (as well as power increases within those regions) during object exploration was that the rats stopped locomoting.

To assess this possibility, power and coherence were calculated for hippocampal LFPs during novel object exploration events (mean number of events ± SEM across rats = 50.8 ± 8.6), stationary moments when the rat was not exploring objects (78.7 ± 26.5), locomotion as a rat approached novel objects (50.8 ± 8.6), and locomotion not close in time to object exploration (168.2 ± 18.9) (see Experimental Procedures for details on how these epochs were defined, and see Figure S1 for confirmation that average speed of movement differed across these four behavioral states). Figure 2 shows subregional power and coherence across the four behavioral conditions (approach, exploration, stationary, and running). The results are also shown after subtracting the grand mean across behavioral conditions to highlight better the similarities and dissimilarities between conditions in a manner that paralleled the statistical testing. Specifically, differences in spectral measures between conditions were evaluated by an ANOVA-based statistical approach that tested whether data from at least one condition differed from the grand mean. Table S1 provides the accompanying statistics for each significant frequency range (frequency cluster) derived from a cluster-based random permutation approach (see Experimental Procedures for details of analyses). Figure S2 reproduces the data displayed in Figure 2 but includes only frequencies below 20 Hz to enhance visualization of differences in this lower frequency range. The results show that hippocampal oscillatory activity during object exploration differed markedly from hippocampal activity during locomotion and, importantly, from hippocampal activity during stationary moments. This latter finding indicates that the hippocampal oscillatory network state during object exploration

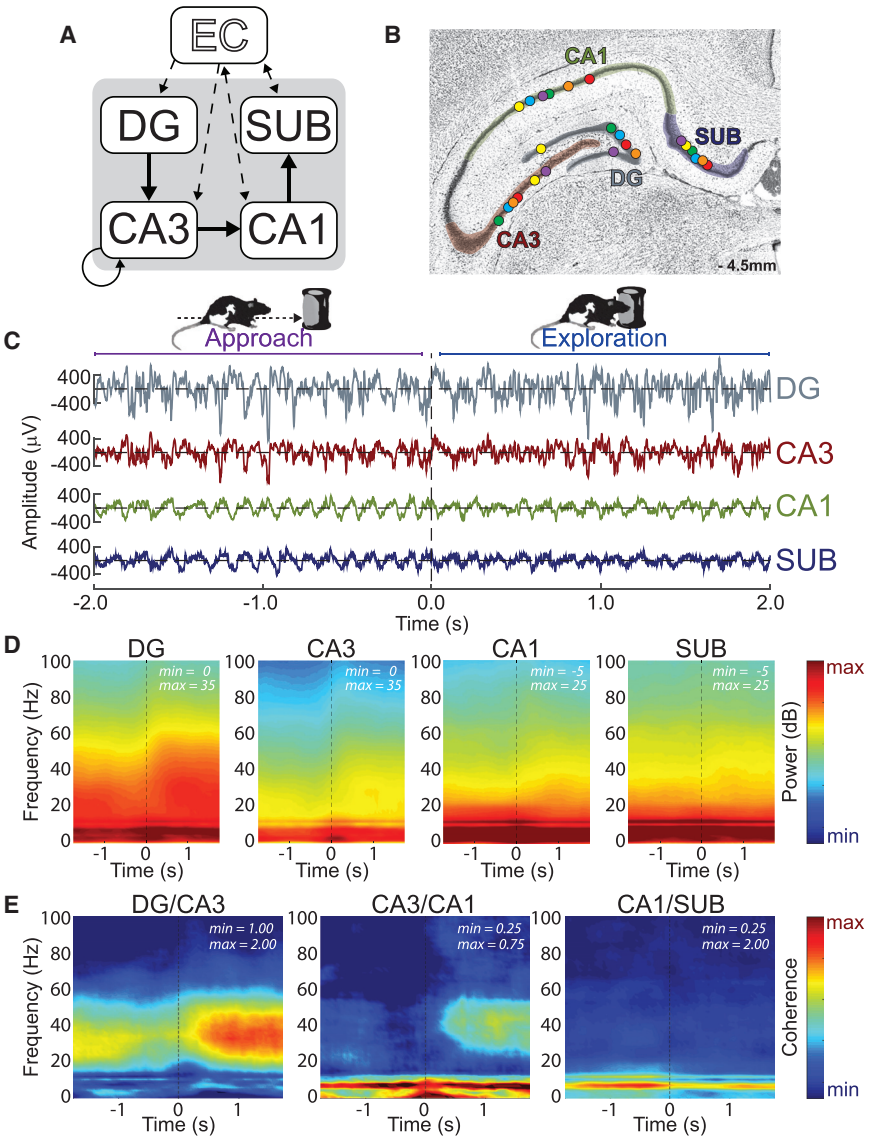

Figure 1. Slow Gamma Coherence Increased while Rats Explored Novel Objects

(A) Illustration of the serial connections of the hippocampal subregions (DG, CA3, CA1, and SUB [subiculum]), as well as its connections with the entorhinal cortex (EC).

(B) Coronal hippocampal section showing LFP recording locations (circles) for each rat (different colors) in each of the four targeted subregions.

(C) Example LFP data as a rat approached (<0 s) and explored (>0 s) a novel object.

(D) Moving window spectrograms for each hippocampal subregion time-locked to the initiation of novel object exploration (0 s). Minimum and maximum power values in decibels are noted on each spectrogram.

(E) Moving window coherograms for each pair of directly connected hippocampal subregions time-locked to the initiation of novel object exploration (0 s). Minimum and maximum coherence values are noted on each coherogram. Increased coherence and power in the slow gamma range were apparent for DG/CA3 and CA3/CA1 during exploration relative to approach.

could not be accounted for merely as a reduction in locomotive speed, instead supporting the idea that hippocampal subregions were engaged in a unique pattern of oscillatory activity that was specific to object exploration.

In particular, object exploration was distinguished from the other behavioral conditions by especially prominent slow gamma (30–55 Hz) and fast gamma (65–90 Hz) power in DG, CA3, and CA1, consistent with a previous report (Trimper et al., 2014). Stationary moments were distinguished by relatively high beta (13–25 Hz) power in DG and CA3, as well as relative decreases in fast gamma power in CA1 and subiculum and in theta power in all four subregions. The oscillatory patterns associated with stationary moments are consistent with previous studies that reported changes associated with cessation of locomotion (Ahmed and Mehta, 2012; Kemere et al., 2013; Zheng et al., 2015), though Rangel et al. (2015) observed increases in DG beta only when cessation of locomotion occurred at behaviorally relevant locations. The two conditions involving locomotion (i.e., approaching an object or running on a track with no object present) were similar to each other and were distinguished from the other conditions by lower levels of (and perhaps somewhat lower-frequency) slow gamma power (relative to object exploration), particularly in DG and CA3, and by high levels of theta power, particularly in CA1 and subiculum. In addition to power, LFP synchrony between connected hippocampal regions, as measured with coherence, also distinguished object exploration from the other behavioral conditions. Object exploration was associated primarily with large relative increases in slow gamma coherence between DG and CA3 and between CA3 and CA1. Stationary moments were associated with relatively high beta coherence between DG and CA3. Theta coherence between CA1 and subiculum was similarly high for both locomotive states relative to the other two behavioral conditions. Thus, distinct overt behaviors were associated with markedly different patterns of oscillatory activity throughout the hippocampal subregions, and the pattern of activity observed during object exploration—namely, prominent slow gamma in DG, CA3, and CA1—could not be accounted for merely as the product of locomotive speed.

Theta, slow gamma, and fast gamma oscillations were prominent in the hippocampal LFPs recorded in the present study, and prior studies of hippocampal oscillations have observed that the amplitude of gamma oscillations can be modulated by the phase of theta oscillations (e.g., Tort et al., 2009; Trimper et al., 2014). We therefore next asked whether the magnitude of the theta-phase modulation of slow gamma or fast gamma

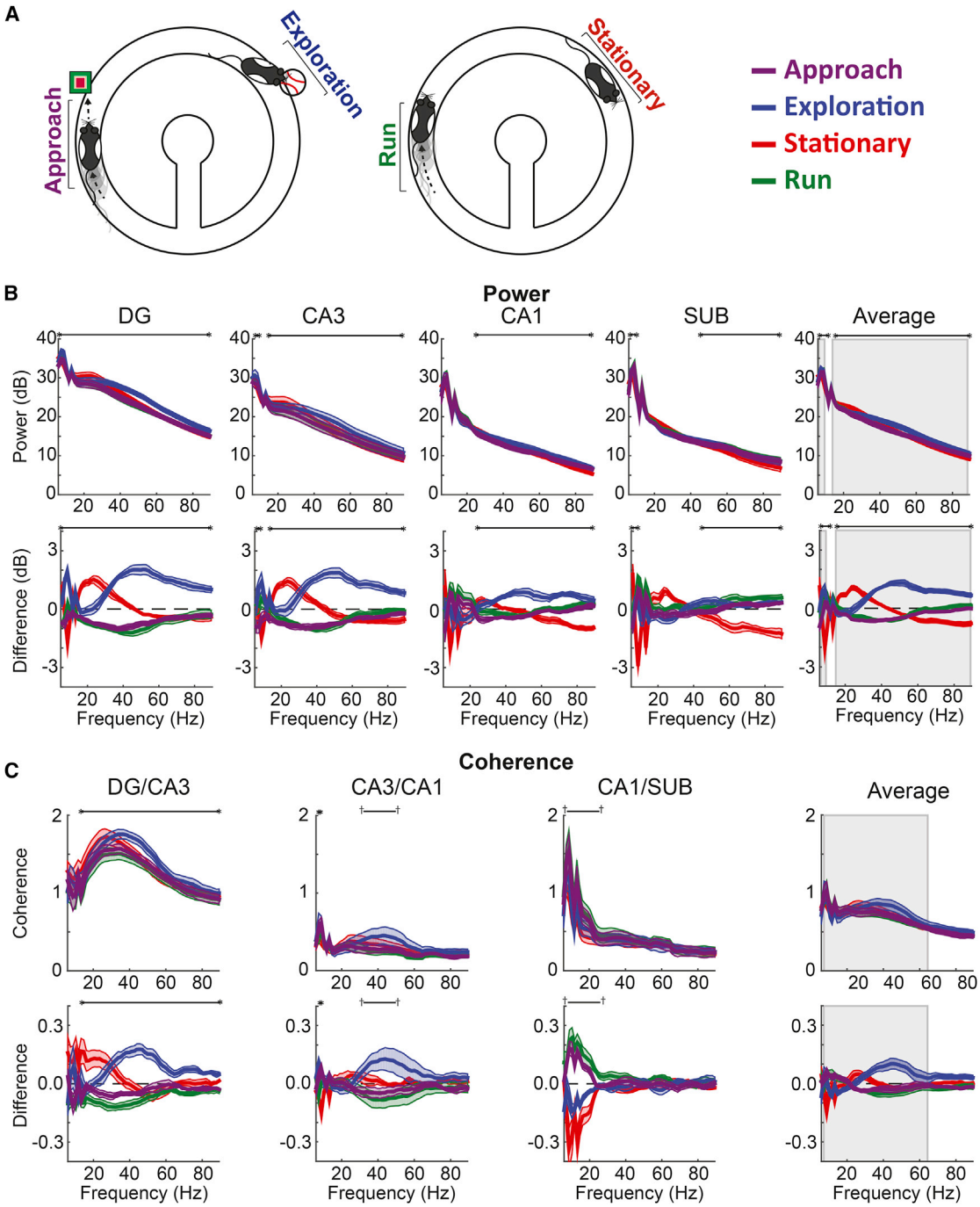

Figure 2. Object Exploration Was Accompanied by a Distinct Spectral Profile

(A) Illustration of the four behavioral states analyzed.

(B) Top: spectral power for each hippocampal subregion (and averaged across subregions) for each behavioral state. Bottom: spectral power plotted as the difference from average across behavioral states.

(C) Top: coherence for each directly connected pair of hippocampal subregions (and averaged across subregion pairs). Bottom: coherence plotted as the difference from average across behavioral states.

Throughout the figure, gray rectangles mark frequency ranges exhibiting significant interactions between behavioral state and subregion. Black horizontal lines bookended by dagger symbols (†) indicate frequency ranges differing significantly ($p < 0.05$) across behavioral states, and those bookended by asterisks indicate significant differences after Bonferroni correction for multiple comparisons (here, 5 for power and 4 for coherence). Colored lines indicate mean (darker shading) ± SEM (lighter shading). See also Figures S1–S3.

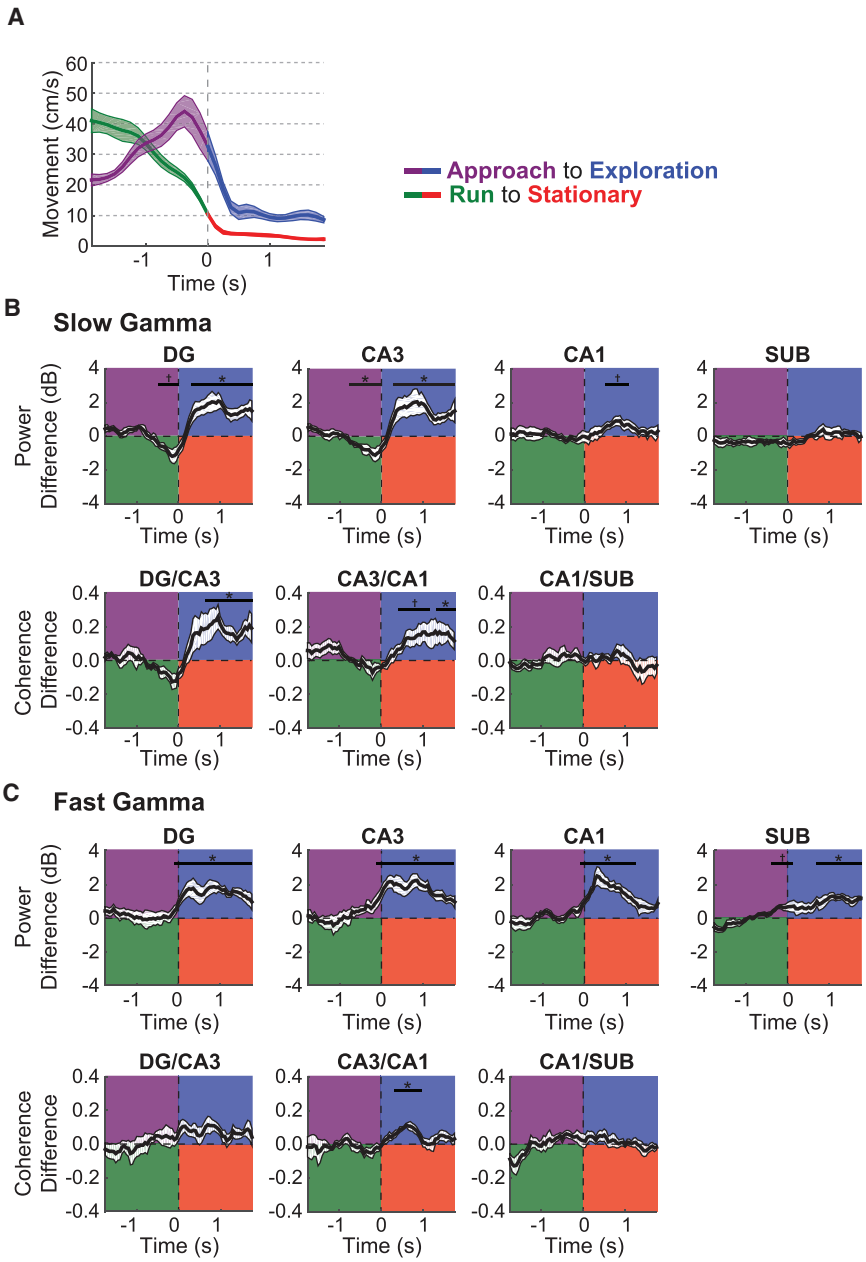

Figure 3. Gamma Power and Coherence during Exploration Were Not Explained as the Products of the Cessation of Locomotion

(A) Speed of movement for 4 s epochs surrounding the transition from novel object approach to exploration (purple to blue) and from run to stationary (green to red).

(B) Slow gamma power (top) and coherence (bottom) plotted as the difference between behavioral state transitions (approach to exploration minus run to stationary). For example, for CA3 slow gamma power, power was reduced for approach relative to run but increased during exploration relative to stationary.

(C) Fast gamma power (top) and coherence (bottom) plotted as the difference between behavioral state transitions (approach to exploration minus run to stationary).

Indicators of statistical significance throughout are the same as in Figure 2, except that Bonferroni correction involved four and three comparisons here for power and coherence, respectively. Colored lines indicate mean (darker shading) ± SEM (lighter shading). See also Tables S1 and S2.

amplitude differed between behavioral conditions in DG, CA3, CA1, or subiculum. The magnitude theta-phase modulation was calculated separately for slow gamma and fast gamma as a modulation index based on the LFP in each region as described previously (e.g., Tort et al., 2009). Figure S3 shows the results as mean modulation indices across rats for each region and for each behavioral condition. The amplitudes of both slow gamma and fast gamma were modulated by the phase of theta oscillations in DG, CA3, CA1, and subiculum, but the modulation indices in each region were similar across behavioral conditions (exploration, stationary, run, and approach). Specifically, one-way ANOVAs for slow gamma and for fast gamma within each region observed no main effects of behavioral condition (all ps > 0.10). Thus, although the patterns of theta and gamma oscillations, as measured by power and coherence, differed across behavioral states, the extent to which slow gamma and fast gamma oscillations were modulated by the phase of theta did not.

As an additional control analysis to rule out cessation of locomotion as the primary driver of the prominent gamma increases during object exploration, slow gamma and fast gamma power and coherence were calculated across time relative to onset of object exploration (mean number of events ± SEM across rats = 50.8 ± 8.6) and to offset of locomotion when no objects were present (i.e., 2 s of locomotion followed by 2 s of remaining stationary; 17.0 ± 4.6 events). Figure 3 shows these data, in addition to differences in average locomotion speed. When rats stopped to explore objects compared to when rats simply stopped, gamma power and coherence, particularly slow gamma in DG and CA3, were markedly and significantly higher (see Table S2 for detailed statistics). The amount of head movement during object exploration was somewhat greater than during stationary moments (Figure 3A), further indicating that the increased slow gamma power and coherence during exploration were not simply related to the negative correlation between movement speed and slow gamma power (e.g., Figure S1). Fast gamma power in all subregions and fast gamma coherence between CA3 and CA1 were also revealed to increase significantly during object exploration. However, these fast gamma differences could

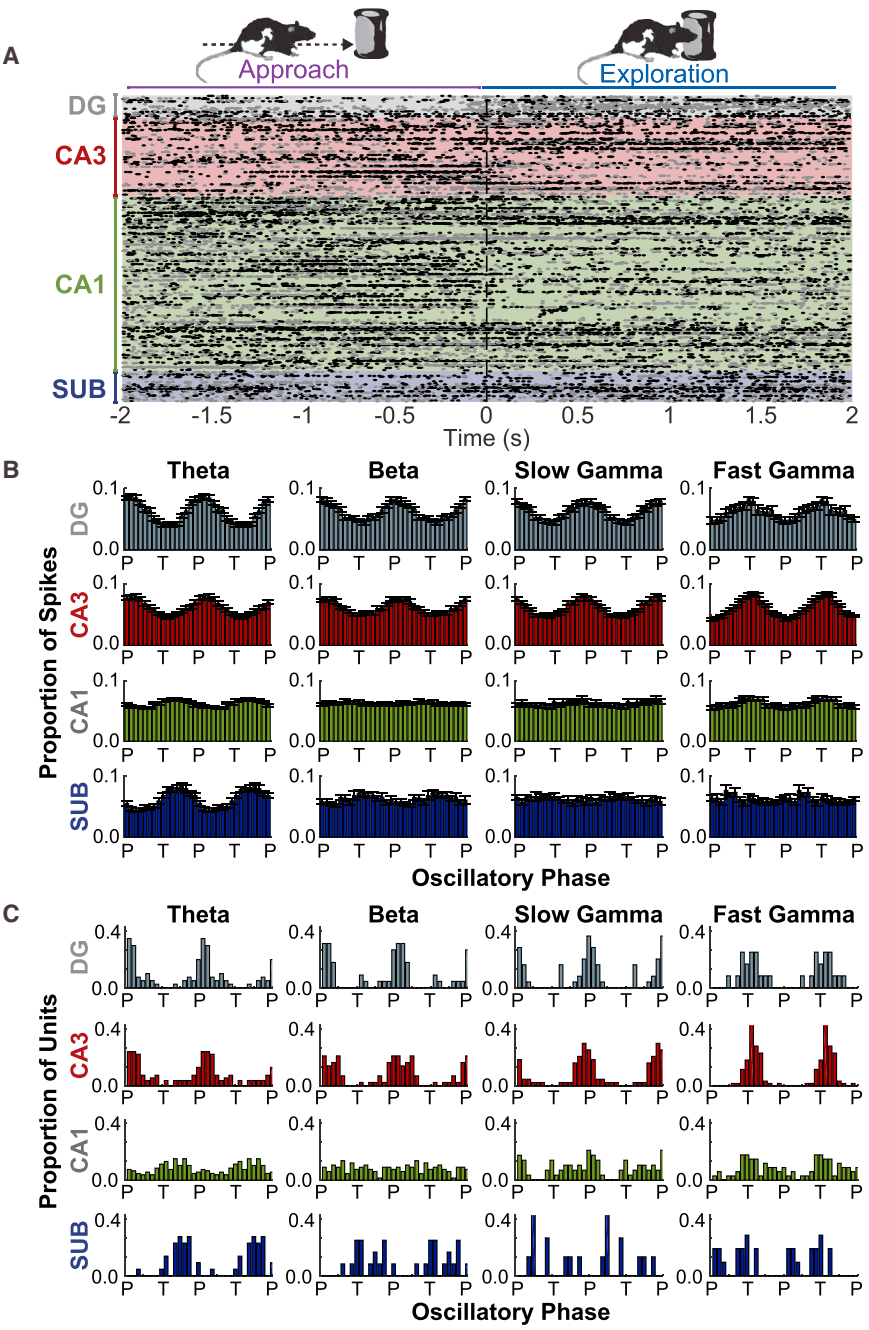

Figure 4. Principal Cell Firing Aligned Strongly to Local Oscillations in Distinct Frequency Bands

(A) Peri-event raster of spike times by subregion time-locked to the initiation of object exploration events (0 s) (approach, <0 s; exploration, >0 s). Each dot indicates an action potential. Each row shows all action potentials from a single neuron. Rows alternate between gray and black dots for better visibility.

(B) Mean distributions of action potentials in each subregion relative to the phase (p, peak; F, falling; T, trough; R, rising) of distinct oscillatory rhythms (denoted at top) recorded from that same subregion. Averages and error (SEM) are for those neurons found to be significantly phase modulated (see text).

(C) Distributions across significantly phase-modulated neurons of the mean preferred oscillatory phase for spiking.

Data are plotted twice in (B) and (C), replicated across the oscillatory cycle, to aid visualization of periodicity. See also Figures S3–S5 and Table S3.

potentially be accounted for by locomotive speed differences. Altogether, these results indicate that the pattern of hippocampal LFP activity during object exploration represents a distinct network state and demonstrate that the high levels of slow gamma oscillations reflect more than the cessation of locomotion.

Hippocampal Spike Timing Was Modulated by Oscillations

An important component of oscillatory analyses is the demonstration of spiking modulation by rhythmic LFP activity, which would indicate that oscillations in LFPs were attributable to local circuits and could not instead be attributed to volume conduction from distal sources (Buzsáki et al., 2012). Therefore, to assess the extent to which oscillations in hippocampal LFPs modulated spike timing within and between subregions, action potentials from principal neurons in each subregion were compared to simultaneously recorded LFPs in each region (e.g., DG spikes and DG LFPs), as well as to simultaneously recorded LFPs in downstream connected regions (e.g., DG spikes and CA3 LFPs). Across the entire recording session, regardless of behavioral state, the overall trend was that spike timing for a substantial portion of neurons in all four subregions (Table S3) was significantly phase aligned to multiple oscillatory ranges (theta, beta, slow gamma, and/or fast gamma), both in the same subregion (Figure 4) and in the immediate downstream region (Figure S4). Only neurons firing at least 50 action potentials when oscillatory power was strong were considered to address the possibility that spike-phase relationships could be obscured by including spikes in the analyses when oscillations were not prominent. The analysis was conducted separately for each frequency range (theta, beta, slow gamma, and fast gamma). The results indicated that the timing of action potentials of principal neurons of the hippocampus were modulated by oscillations in each frequency range but that the extent of modulation depended on the specific range and hippocampal subregion. In addition, the phase at which spiking tended to

occur relative to oscillations in the LFP depended on the specific frequency range and hippocampal subregion (Figures 4 and S4). In particular, action potentials of significantly phase-modulated principal cells in DG and CA3 were both more likely to be aligned to the peak of local slow gamma oscillations yet both more likely to be aligned to the trough of local fast gamma oscillations (Watson-Williams F test of phases for slow gamma versus fast gamma; DG: $F(1,47) = 76.35$, $p < 0.0001$; CA3: $F(1,137) = 318.5$, $p < 0.0001$). More broadly, the findings suggest that the LFP oscillations reflect physiologically relevant signals in the hippocampus.

In comparison to LFP oscillations, hippocampal spiking activity as measured by either firing rates (Figure S5) or spike-phase timing (Figures 4 and S4) only modestly distinguished behavioral states, perhaps reflecting an advantage for LFPs in summing activity across many neurons to assess network states (Buzsáki et al., 2012). In particular, a significant difference in firing rate across behaviors, after Bonferroni alpha correction for four subregions, was revealed in CA1 ($n = 266$, $F(3,795) = 18.65$, $p = < 0.0001$, partial $eta^2 = 0.066$) and DG ($n = 40$, $F(3,117) = 4.356$, $p = 0.006$, partial $eta^2 = 0.006$), but not in CA3 ($n = 124$, $F(3,369) = 2.263$, $p = 0.081$, partial $eta^2 = 0.0181$) or subiculum ($n = 39$, $F(3,114) = 0.721$, $p = 0.542$, partial $eta^2 = 0.019$). Modestly higher CA1 pyramidal neuron firing rates were associated with locomotion, consistent with previous reports (e.g., Ahmed and Mehta, 2012; Zheng et al., 2015), whereas putative DG granule cells preferably fired during exploration relative to other behavioral states.

In terms of spike-phase timing, low hippocampal firing rates overall (mean hertz ± SEM: DG = 0.79 ± 0.12, CA3 = 0.63 ± 0.07, CA1 = 0.87 ± 0.45, subiculum [SUB] = 1.09 ± 0.12) prevented analyses regarding differences in spike timing across behavioral conditions for ranges other than the theta range, because spike-phase modulation by transient or nonstationary rhythms can be assessed only when spikes are present and oscillatory bouts are pre-selected to be strong to avoid spurious results (Colgin et al., 2009). These analyses of spike to theta phase modulation by behavioral state (Figure S5) revealed no significant differences in terms of the number of significantly phase-modulated neurons across states, at least not after Bonferroni correction for four subregions (DG: $\chi^2(3) = 5.946$; CA3: $\chi^2(3) = 8.682$, $p = 0.035$; CA1(3): $\chi^2(3) = 03.316$, $p = 0.345$; SUB: $\chi^2(3) = 4.110$, $p = 0.250$), but did show a significant increase in the strength of theta phase alignment (i.e., pairwise phase consistency) (Vinck et al., 2010) for locomotive relative to nonlocomotive states for DG ($F(3,53) = 7.02$, $p < 0.001$, partial $eta^2 = 0.397$). Thus, spiking in all hippocampal regions was modulated by oscillations in all four oscillatory ranges (Figure 4), but analytical constraints permitted assessment of spike-phase differences between behavioral conditions for only the theta range. As a result, subsequent analyses focused on whether oscillations in LFPs across subregions of the hippocampus during object exploration reflected memory for the encounters or just the behavioral state of exploration, an approach that revealed marked oscillatory differences during object exploration (Figures 1, 2, and 3) and that was not limited by the analytical constraints that pertained to spiking.

Hippocampal Slow Gamma Oscillations during Object Exploration Distinguished Memory Conditions in an Object-Location Associative Memory Task

A main question of the present study was whether patterns of hippocampal oscillations would correspond to associative memory for the object encounters. Figure 5 shows a schematic of and behavioral results from the object-location recognition memory task, which involved up to 24 trials per session of rats completing triplets of clockwise laps on a circle track and spontaneously exploring novel objects, objects repeated in the same location, and objects repeated in swapped locations. Rats exhibit a well-known preference for novelty (Ennaceur and Delacour, 1988); thus, a reduction in exploration time across successive encounters with a stimulus can be interpreted as rats remembering the stimulus. Rats showed a large and significant reduction in exploration duration ($t(5) = 4.50$, $p = 0.006$, Cohen's $d = 1.836$) when novel objects from lap 1 were encountered again in the same locations on lap 2 (mean number of events ± SEM across rats = 87.0 ± 10.1), which indicated memory for at least the object identities. To ask whether the rats also remembered the specific locations of the objects, on some trials, the objects were repeated again in swapped locations on lap 3. Rats explored these swapped objects (mean number of events ± SEM across rats = 80.7 ± 5.6) for a different amount of time than repeated (20.3 ± 1.4 events) or novel objects ($n = 20.3 \pm 1.4$ events) in control conditions ($F(2,10) = 10.93$, $p = 0.003$, partial $eta^2 = 0.686$). Specifically, rats explored swapped objects for a longer duration than objects repeated in the same location ($t(5) = 3.45$, $p = 0.018$, $d = 1.41$) but less than novel objects on lap 3 ($t(5) = 3.20$, $p = 0.024$, $d = 1.30$), indicating that rats had memory for the prior locations of objects, similar to previous reports (e.g., Save et al., 1992).

To ask whether hippocampal oscillations might differ by memory condition, power and coherence across subregions were calculated during the first second of lap 3 object exploration of repeated, novel, and swapped objects lasting at least 1 s, when overt movement was similar (Figure S1). A window of 1 s, rather than a longer duration (e.g., 2 s), was selected to permit inclusion of a number of events from each condition in the analyses (mean number of events ± SEM across rats = 10.0 ± 1.1, 4.2 ± 0.9, and 27.8 ± 4.9 for novel objects, repeated objects, and swapped objects on lap 3, respectively). Figure 6 shows the results across frequency ranges as differences from the grand mean across conditions to highlight the comparisons of interest (see Table S4 for detailed statistics; see Figure S6 for figures that include individual data points for each rat). Slow gamma power in DG and CA3 differed markedly across the three memory conditions, in both cases being at its relative highest during exploration of novel objects, its relative lowest during exploration of repeated objects, and at an intermediate level during exploration of swapped objects. Based on the overall prominence of hippocampal gamma oscillations during object exploration (e.g., Figure 2), power in each subregion was also averaged and plotted separately in the slow gamma range and fast gamma range as normalized differences across the three memory conditions. Statistically significant linear trends (novel > swap > repeat) were observed for overall average hippocampal slow gamma power ($F(1,5) = 15.60$, $p = 0.011$,

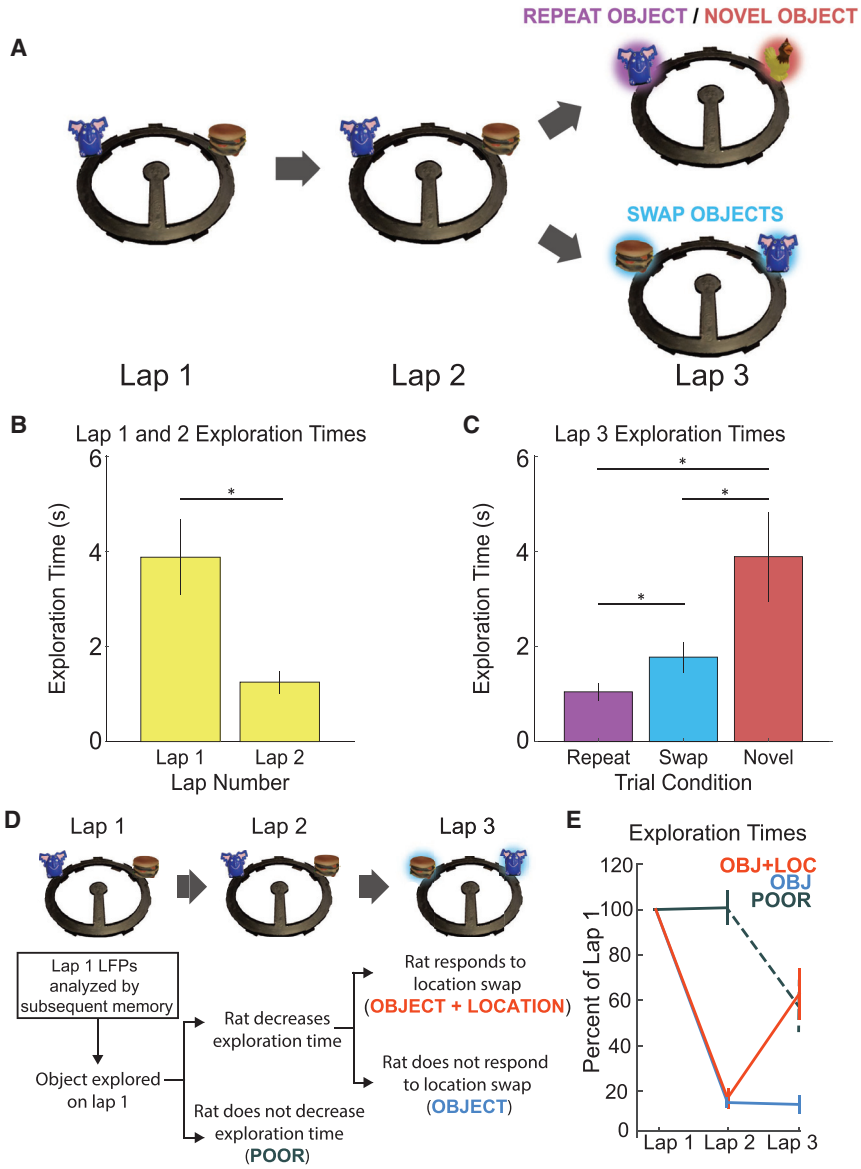

Figure 5. Rats Demonstrated Memory for Objects and Objects' Locations

(A) Schematic of the memory task. Each trial consisted of three laps around a circular track. On lap 1 of each trial, rats encountered two novel objects. On lap 2, rats encountered duplicates of those same two objects in the same positions. On lap 3, one of two trial-type manipulations was presented: (1) one object was replaced with a duplicate while the other object was replaced by a novel object (repeat object/novel object trial) or (2) the objects were replaced by duplicates in swapped locations (swap objects trial).

(B) A significant reduction in average exploration time from lap 1 to lap 2 evidenced rats' memory for the novel objects presented on lap 1. Asterisks indicate $p < 0.05$.

(C) On lap 3, rats explored novel objects longer than swap objects and swap objects longer than repeat objects, indicating memory for the objects' locations. Asterisks indicate $p < 0.05$.

(D) Diagram of how object+location, object, and poor subsequent memory conditions were defined (also see Experimental Procedures).

(E) Average exploration times across laps sorted by subsequent memory conditions and plotted as the percentage of lap 1 exploration time using the colors indicated in (D). Error bars throughout the figure show SEM across rats.

partial eta^2 = 0.757) and specifically for DG slow gamma power ($F(1,5) = 28.46$, $p = 0.003$, partial eta^2 = 0.851) and CA3 slow gamma power ($F(1,5) = 16.80$, $p = 0.009$, partial eta^2 = 0.771), whereas no significant differences were observed for any contrast in the fast gamma range (see Figure 6 and Table S5 for statistical details).

Compared to the results for power, coherence between connected hippocampal subregions showed relatively small differences across memory conditions, at least when plotted across a range of frequencies (Figure 6). However, when coherence between subregions was averaged across the slow gamma range, statistically significant linear trends (novel > swap > repeat) were observed for overall hippocampal slow gamma coherence ($F(1,5) = 11.85$, $p = 0.018$, partial eta^2 = 0.703), as well as specifically for the slow gamma coherence between CA1 and subiculum ($F(1,5) = 6.70$, $p = 0.046$, partial eta^2 = 0.583). To ask whether these results for coherence could be explained by simultaneous but undirected increases in slow gamma power (e.g. because of volume conduction) the non-normalized directed transfer function (DTF) was calculated and plotted for oscillatory interactions between hippocampal subregions for the three memory conditions. DTF is a directional autoregressive metric (similar to Granger causality in the frequency domain) that discounts zero-lag phase relationships and instead reflects the predictiveness of oscillations in one region for oscillations of the same frequency in another region (Kamiński and Blinowska, 1991). Statistically significant linear trends (novel > swap > repeat) were observed for overall hippocampal slow gamma DTF ($F(1,5) = 19.01$, $p = 0.007$, partial eta^2 = 0.795), as well as specifically for the DTF between DG and CA3 ($F(1,5) = 8.01$, $p = 0.037$, partial eta^2 = 0.616). No significant differences between memory conditions were observed in the fast gamma range for power, coherence, or DTF (zero of thirteen linear contrasts in Figures 6C–6E; see Table S5 for detailed statistics). In contrast, seven of the thirteen linear contrasts for slow gamma power, coherence, and DTF (Figures 6C–6E) were statistically significant, a proportion higher than one would expect by chance with an alpha level of 0.05 (see Figure 6 for clarification of alpha corrections for multiple comparisons).

Thus, the results demonstrated increased slow gamma activity in a subset of hippocampal subregions correlated with the

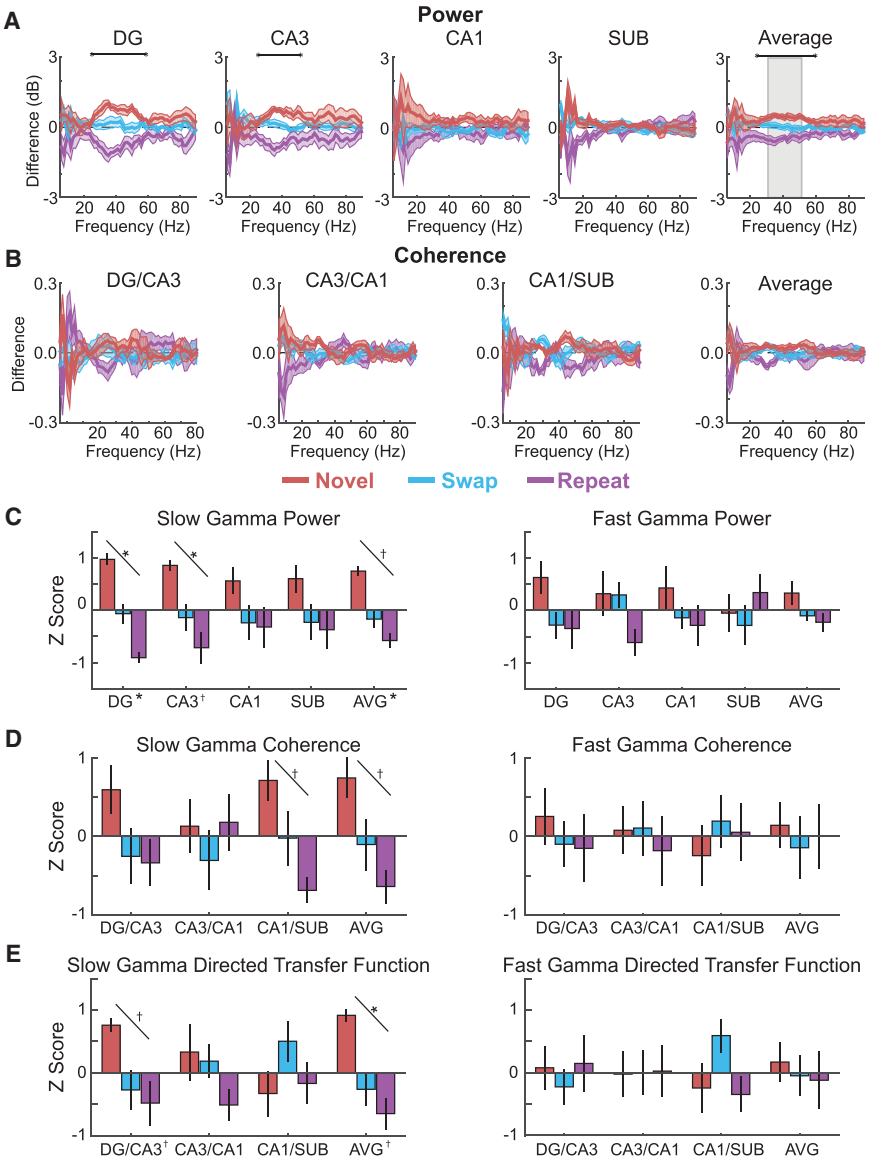

Figure 6. Slow Gamma during Lap 3 Object Exploration Related to Object-Location Memory Condition

(A) Power by subregion (and the average across subregions) plotted as the difference from mean across memory conditions (denoted throughout the figure by colors indicated in the legend).

(B) Coherence for each directly connected subregion pair plotted as the difference from mean across conditions.

(C) Average slow gamma and fast gamma power for each subregion (and averaged across subregions [AVG]) standardized to the mean across conditions and plotted as the *Z* score.

(D) Average slow gamma and fast gamma coherence for each directly connected subregion pair (and averaged across subregion pairs [AVG]) standardized to the mean across conditions and plotted as the *Z* score.

(E) Average slow gamma and fast gamma non-normalized directed transfer function standardized to the mean across conditions and plotted as the *Z* score.

Colored lines in (A) and (B) indicate mean (darker shading) ± SEM (lighter shading). Error bars in (C)–(E) show SEM. Indicators of statistical significance in (A) and (B) are the same as in Figure 2. Similarly, diagonal lines in (C)–(E) indicate statistical significance of linear trends, and symbols next to the region labels on the x axes indicate statistical significance for that region of one-way repeated-measures ANOVAs across object conditions. See also Figure S6 and Tables S4 and S5 for detailed statistics.

degree of novelty associated with the lap 3 object presentations. In particular, novel objects were associated with the largest slow gamma amplitude, synchrony, and predictiveness. In comparison, repeated objects in novel locations were associated with the second-highest levels, and repeated objects in repeated locations were associated with the lowest levels. These results support a role for hippocampal slow gamma oscillations in the encoding of novel associative recognition memories for objects and their locations.

Hippocampal Slow Gamma Oscillations during Exploration of Novel Objects Related to Subsequent Memory for Objects and Locations

The pattern of slow gamma differences observed during the lap 3 test of object-location associative memory (novel > swap > repeat) suggested that the degree of slow gamma might have been inversely related to the amount of information repeated from the initial object presentation and thus perhaps positively related to the amount of new encoding at the time of the test. To ask more directly whether hippocampal oscillations would reflect memory encoding, LFPs recorded during lap 1 novel object exploration were split into three subsequent memory conditions based on whether, on laps 2 and 3, the rats showed good memory for both the object and its location (object+location); good memory for the object, but not its location (object); or poor memory for both aspects of the initial encounter (poor). Figure 5 illustrates how the memory conditions were defined and shows performance split by the three subsequent memory conditions. Rats did not decrease their exploration times from lap 1 to lap 2 for the poor memory condition ($t(5) = 0.296$, $p = 0.779$, $d = 0.121$) but decreased their exploration times from lap 1 to lap 2 similarly for object+location (83% reduction; $t(5) = 21.857$, $p < 0.0001$, $d = 8.923$) and object (85% reduction; $t(5) = 51.627$, $p < 0.0001$, $d = 21.08$) memory conditions. On lap 3, rats significantly increased their exploration times for the object+location condition (lap 2 to lap 3 percentage increase = 341%; $t(5) = -3.425$, $p = 0.019$, $d = 1.398$) but did not do so for the object memory condition (lap 2 to lap 3 percentage

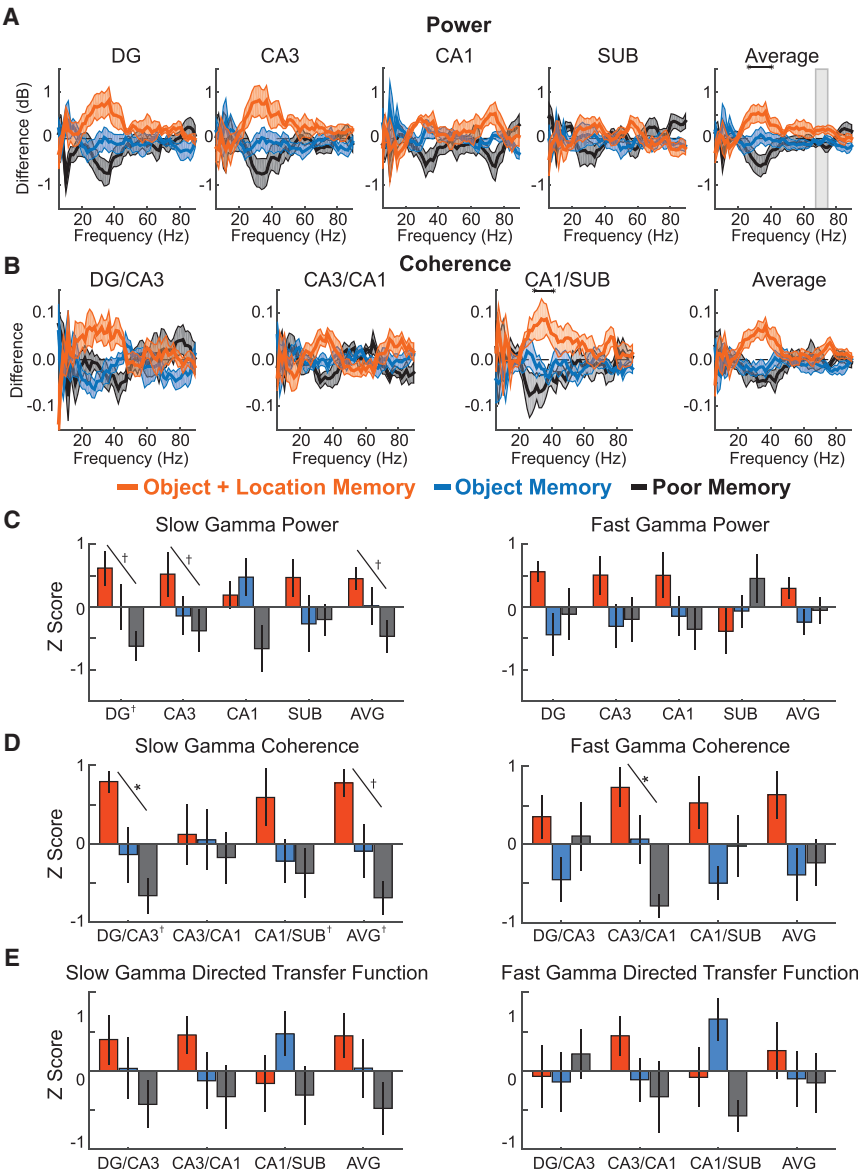

Figure 7. Slow Gamma during Novel Object Exploration Related to Subsequent Object-Location Associative Memory

(A) Power by subregion (and the average across subregions) plotted as the difference from mean across memory conditions (denoted throughout the figure by colors indicated in the legend).

(B) Coherence for each directly connected subregion pair plotted as the difference from mean across conditions.

(C) Average slow gamma and fast gamma power for each subregion (and averaged across subregions [AVG]) standardized to the mean across conditions and plotted as the *Z* score.

(D) Average slow gamma and fast gamma coherence for each directly connected subregion pair (and averaged across subregion pairs [AVG]) standardized to the mean across conditions and plotted as the *Z* score.

(E) Average slow gamma and fast gamma non-normalized directed transfer function standardized to the mean across conditions and plotted as the *Z* score.

Colored lines in (A) and (B) indicate mean (darker shading) ± SEM (lighter shading). Error bars in (C)–(E) show SEM. Indicators of statistical significance in (A) and (B) are the same as in Figure 2. Similarly, diagonal lines in (C)–(E) indicate statistical significance of linear trends, and symbols next to the region labels on the x axes indicate statistical significance for that region of one-way repeated-measures ANOVAs across object conditions. See also Figure S7 and Tables S6 and S7 for detailed statistics.

decrease = 5%; t(5) = 0.304, p = 0.773, d = 0.124). Thus, the behavioral results validated the partitioning of the events into poor, object, and object+location conditions.

Figure 7 shows differences during the initial 1.5 s of novel object exploration between subsequent memory conditions for power, coherence, and DTF across hippocampal subregions (see Tables S6 and S7 for detailed statistics; see Figure S7 for figures that include individual data points for each rat). A 1.5 s window was used rather than a 2 s window to permit inclusion of enough events in each memory condition (mean number of events ± SEM across rats = 8.5 ± 1.6, 21.5 ± 3.7, and 8.8 ± 2.1 for object+location, object, and poor memory conditions, respectively). Similar to the results for the lap 3 memory test, the subsequent memory contrasts highlighted the slow gamma range. More specifically, average power in the slow gamma range in DG and CA3 differed markedly and statistically significantly across the three memory conditions. For both subregions, slow gamma power was at its relative highest during exploration of novel objects for which both the object and the location were subsequently remembered, its relative lowest during exploration of novel object encounters that were poorly remembered, and at an intermediate level during exploration of novel objects for which the object identity, but not the location, was remembered (linear trend; DG: F(1,5) = 11.64, p = 0.019, partial eta^2 = 0.699; CA3: F(1,5) = 6.835, p = 0.047, partial eta^2 = 0.578; overall hippocampus mean: F(1,5) = 6.835, p = 0.047). This same pattern (object+location > object > poor) was also present in DG-CA3 coherence (F(1,5) = 40.294, p = 0.001, partial eta^2 = 0.890) and overall hippocampal coherence (F(1,5) = 14.410, p = 0.013, partial eta^2 = 0.742). The pattern was similar for DTF, although in this case the differences did not reach statistical significance (all ps > 0.142). In comparison, for the fast gamma range, the trends for power, coherence, and DTF were less consistent and were statistically significant for only CA3-CA1 coherence (F(1,5) = 15.981, p = 0.010, partial eta^2 = 0.762). Altogether, five of the thirteen linear contrasts for slow gamma power, coherence, and DTF were statistically

significant, a proportion higher than one would expect by chance with an alpha level of 0.05 (Figures 7C–7E).

Thus, combined with the previous results from the lap 3 memory test, the results from lap 1 novel object exploration indicated that the patterns of oscillations in the hippocampus, particularly in the slow gamma range, clearly distinguished moments when the rats were similarly engaged in the behavior of object exploration based on inferred differences in subsequent memory content and quality. In particular, the amount or success of memory encoding during an object-location associative memory task appeared to be reflected in the general prominence of intra-hippocampal slow gamma oscillatory interactions.

DISCUSSION

In the present work, we asked whether the patterns of hippocampal oscillations during object exploration in an object-location associative memory task corresponded best to (1) cessation of locomotion, (2) the act of object exploration, or (3) memory for the object encounters. Results indicated that the overall pattern of hippocampal theta, beta, slow gamma, and fast gamma oscillations across DG, CA3, CA1, and subiculum were influenced by all three variables. However, during object exploration, slow gamma oscillations in particular related most specifically to associative memory for the object encounters. Hippocampal LFPs during object exploration were marked by prominent slow gamma oscillations, for which the strength and degree of intra-hippocampal synchrony related to subsequent spatial associative memory for the objects and, likewise, differentiated among bouts of exploring novel, repeated, and relocated objects. These patterns of slow gamma oscillations differed starkly from those observed during both locomotion and stationary moments. The memory effects on slow gamma oscillations were not limited to oscillatory power in a single hippocampal subregion or to coherence in any one region-region interaction but instead appeared to reflect an increased prevalence of slow gamma oscillations throughout the hippocampus (although not uniformly) during associative memory encoding. Thus, the overall pattern of oscillatory activity in the hippocampus distinguished object exploration as a unique network state, and the specific pattern of hippocampal slow gamma oscillations reflected associative memory for the encounters rather than solely the act of exploration.

One interpretation of the current results is that slow gamma oscillations related specifically to associative encoding of object-location memory in the hippocampus, whereas the other patterns of oscillations, particularly theta, reflected more global interactions between the hippocampus and other brain regions in support of integrating nonmemory processes. Previous studies have highlighted slow gamma oscillations in the hippocampus as an indicator of intra-hippocampal synchrony (Colgin et al., 2009; Colgin and Moser, 2010), and a number of studies have highlighted the importance of the hippocampus for spatial associative memory (e.g., Eichenbaum et al., 1999; Komorowski et al., 2009; Tort et al., 2009). In line with these results, prominent intra-hippocampal slow gamma oscillations during exploration of novel objects related to good subsequent memory for both the object and its location and, at test, correlated with the degree of object or location novelty. Oscillations in other frequency ranges were better explained by differences in overt behavior. Theta oscillations are believed to emerge from, and in turn support, interactions between the hippocampus and many other brain regions (Buzsáki, 2002; Colgin, 2016), and theta rhythms within the hippocampal formation are well known to be strongly modulated by locomotive speed (Bender et al., 2015; King et al., 1998; Sławińska and Kasicki, 1998; Whishaw and Vanderwolf, 1973).

The idea offered here is not that theta and slow gamma oscillations in the hippocampus relate narrowly or universally, for example, to locomotion and associative memory encoding, respectively. Numerous past studies have linked hippocampal theta oscillations and memory performance, for example, during spatial navigation (Belchior et al., 2014; McNaughton et al., 2006; Siegle and Wilson, 2014; Wang et al., 2015; Winson, 1978), and in the current report, we replicate a clear (inverse) relationship between locomotion and slow gamma oscillations in the rat hippocampus. Furthermore, others have previously made the case that slow gamma oscillations in the hippocampus correspond to memory retrieval processes rather than encoding processes (Colgin et al., 2009; Colgin and Moser, 2010). Instead, the view advanced here is that memory states intersect with behavioral states to shape the oscillatory dynamics of the hippocampus. By this view, during encounters with novel objects—and against the backdrop of oscillations corresponding to that behavioral state—slow gamma oscillations could coordinate spike timing and synaptic plasticity between subregions of the hippocampus in support of associating those objects in memory with the location in which it was encountered as the rats navigated and explored the entire testing apparatus.

More broadly, the current findings highlight the importance of considering object exploration as something more than the cessation of locomotion and how memory for this behavior would be supported by the hippocampus. Many have emphasized the confluence of spatial and nonspatial inputs in the mammalian hippocampus (Knierim et al., 2006; Manns and Eichenbaum, 2006; Witter et al., 2000) and have suggested that it may be particularly important for remembering nonspatial items in a spatial context, such as remembering an object encountered in a particular location (Burgess et al., 2002; Kesner et al., 2004; Jarrard, 1993; Malkova and Mishkin, 2003). Moving forward, additional work will be needed to understand how oscillatory interactions between the hippocampus and other brain regions mediate local and global neural processes needed to negotiate bilaterally between making memories during action and acting on retrieved memories. In this avenue, study of oscillations in the hippocampus can reveal more broadly how action and cognition can combine to shape network dynamics in the brain.

EXPERIMENTAL PROCEDURES

Subjects

Subjects were six male Long-Evans rats aged 6 to 12 months, individually housed (12 hr light/dark cycle, testing during light phase) with free access to water. Rats were placed on a restricted diet such that the animals maintained at least 90% of their free-feeding weight (~400 g). All procedures involving rats were approved by the Institutional Animal Care and Use Committee at Emory

University. The Supplemental Experimental Procedures contain additional details for procedures described here.

Behavioral Task and Analyses

Figure 5 shows a schematic of the behavioral task. Each trial consisted of a single lap around the track with no objects present followed by three laps with objects present in the 10 o'clock and 2 o'clock positions, relative to the inner stem of the track at 6 o'clock. On the first object lap (lap 1), rats encountered two novel objects. On lap 2, rats encountered duplicates of the same objects from lap 1 in the same positions. On lap 3, rats encountered one of two new object configurations. Either one object was replaced with a duplicate in the same location (repeat) while the other was replaced with a novel object (novel), or the two objects were repeated again but in swapped locations (swap). Rats performed up to 72 trials across up to 5 days of testing, with up to 24 trials on a single day. Sessions were recorded using a digital video camera (30 frames/s), and the rat's head location was recorded for each frame. This frame-by-frame location information was combined with manual coding of object exploration events to define epochs of exploration, stationary moments, and periods of locomotion across a range of movement speeds.

The behavioral data were also used to partition lap 1 exploration events by subsequent memory (Figure 5). Specifically, lap 1 object encounters lasting at least 1.5 s were sorted into memory conditions by subsequent exploration times on laps 2 and 3. Objects for which rats reduced their exploration duration from lap 1 to lap 2 by less than 50% were assigned to the poor memory condition. Objects for which rats reduced their exploration from lap 1 to lap 2 by at least 50% and then explored that object more than repeated objects on lap 3 when it swapped locations were assigned to the object+location memory condition. If rats reduced their exploration of an object from lap 1 to lap 2 by at least 50%, but then explored the object on lap 3 less than their average exploration time for repeat objects, the object was assigned to the object memory condition. Lap 3 exploration was compared to the average exploration duration for repeat objects based on the idea that the lap 3 repeat exploration duration would, on average, represent a combination of object+location memories and object memories.

Surgical Implantation of Tetrodes and Data Acquisition

Sterile-tip surgery was conducted under isoflurane anesthesia to implant chronic recording tetrodes, which were subsequently positioned in the principal cell layers of DG, CA3, CA1, and subiculum subregions of the dorsal hippocampus in one hemisphere. LFPs were recorded continuously (sampling rate = 1,500 Hz, bandpass filter = 1–400 Hz). Spiking data were recorded (sampling rate = 30,000 Hz, bandpass = 600–6,000 Hz) for putative action potentials that surpassed a user-defined amplitude threshold. Action potentials recorded on the same tetrode were later manually separated into distinct units by plotting several waveform characteristics across the four wires (e.g., peak spike amplitude, waveform shape as reflected in principal-component analysis) using Offline Sorter (Plexon).

Neural Data Analyses

LFP Analyses

Spectral analyses implemented a multitaper fast Fourier transform method for calculating coherence and power (Bokil et al., 2010). Evaluation of statistically significant differences across conditions and subregions or subregion pairs in spectral measures by frequency was performed using a cluster-based permutation approach similar to that described previously (Maris and Oostenveld, 2007) but adapted here to calculate F statistics (ANOVA) for more than a single independent variable and more than two levels of each variable. Nonnormalized directed transfer function, also referred to as the transfer matrix (H), was calculated as the inverse of the fast Fourier-transformed multivariate autoregressive coefficient matrix (Kamiński and Blinowska, 1991).

Spiking Analyses

For all spiking analyses, only putative pyramidal neurons (n = 448, 424, and 59 for CA3, CA1, and subiculum, respectively) or granule neurons (n = 104 for DG) emitting at least 50 spikes across conditions were considered. Spike-LFP phase analyses were based on procedures in prior reports (Colgin et al., 2009; Mizuseki et al., 2012). In addition, strength of phase modulation was assessed with pairwise phase consistency (Vinck et al., 2010), which quantifies the consistency of angular phase preference for each possible pair of action potentials, thus avoiding the bias associated with mean resultant length.

SUPPLEMENTAL INFORMATION

Supplemental Information includes Supplemental Experimental Procedures, seven figures, and seven tables and can be found with this article online at https://doi.org/10.1016/j.celrep.2017.10.123.

AUTHOR CONTRIBUTIONS

J.B.T. and J.R.M. designed experiments and analyses. J.B.T. conducted experiments and analyses. C.R.G. and K.M. assisted with data collection. A.C.J. and K.M. assisted with data processing. J.B.T. and J.R.M. wrote the manuscript.

ACKNOWLEDGMENTS

We thank Max Farina for his assistance. This work was supported in part by NIH F31 grant MH102956 to J.B.T.

Received: March 10, 2017
Revised: September 1, 2017
Accepted: October 29, 2017
Published: November 28, 2017

REFERENCES

Ahmed, O.J., and Mehta, M.R. (2012). Running speed alters the frequency of hippocampal gamma oscillations. J. Neurosci. *32*, 7373–7383.

Amaral, D.G., and Witter, M.P. (1989). The three-dimensional organization of the hippocampal formation: a review of anatomical data. Neuroscience *31*, 571–591.

Belchior, H., Lopes-Dos-Santos, V., Tort, A.B., and Ribeiro, S. (2014). Increase in hippocampal theta oscillations during spatial decision making. Hippocampus *24*, 693–702.

Bender, F., Gorbati, M., Cadavieco, M.C., Denisova, N., Gao, X., Holman, C., Korotkova, T., and Ponomarenko, A. (2015). Theta oscillations regulate the speed of locomotion via a hippocampus to lateral septum pathway. Nat. Commun. *6*, 8521.

Bokil, H., Andrews, P., Kulkarni, J.E., Mehta, S., and Mitra, P.P. (2010). Chronux: a platform for analyzing neural signals. J. Neurosci. Methods *192*, 146–151.

Brovelli, A., Ding, M., Ledberg, A., Chen, Y., Nakamura, R., and Bressler, S.L. (2004). Beta oscillations in a large-scale sensorimotor cortical network: directional influences revealed by Granger causality. Proc. Natl. Acad. Sci. USA *101*, 9849–9854.

Burgess, N., Maguire, E.A., and O'Keefe, J. (2002). The human hippocampus and spatial and episodic memory. Neuron *35*, 625–641.

Buzsáki, G. (2002). Theta oscillations in the hippocampus. Neuron *33*, 325–340.

Buzsáki, G., Anastassiou, C.A., and Koch, C. (2012). The origin of extracellular fields and currents—EEG, ECoG, LFP and spikes. Nat. Rev. Neurosci. *13*, 407–420.

Clark, R.E., and Squire, L.R. (2010). An animal model of recognition memory and medial temporal lobe amnesia: history and current issues. Neuropsychologia *48*, 2234–2244.

Colgin, L.L. (2016). Rhythms of the hippocampal network. Nat. Rev. Neurosci. *17*, 239–249.

Colgin, L.L., and Moser, E.I. (2010). Gamma oscillations in the hippocampus. Physiology (Bethesda) *25*, 319–329.

Colgin, L.L., Denninger, T., Fyhn, M., Hafting, T., Bonnevie, T., Jensen, O., Moser, M.B., and Moser, E.I. (2009). Frequency of gamma oscillations routes flow of information in the hippocampus. Nature *462*, 353–357.

Davachi, L. (2006). Item, context and relational episodic encoding in humans. Curr. Opin. Neurobiol. *16*, 693–700.

Eichenbaum, H., Dudchenko, P., Wood, E., Shapiro, M., and Tanila, H. (1999). The hippocampus, memory, and place cells: is it spatial memory or a memory space? Neuron *23*, 209–226.

Engel, A.K., and Fries, P. (2010). Beta-band oscillations—signalling the status quo? Curr. Opin. Neurobiol. *20*, 156–165.

Engel, A.K., Fries, P., and Singer, W. (2001). Dynamic predictions: oscillations and synchrony in top-down processing. Nat. Rev. Neurosci. *2*, 704–716.

Ennaceur, A., and Delacour, J. (1988). A new one-trial test for neurobiological studies of memory in rats. 1: behavioral data. Behav. Brain Res. *31*, 47–59.

Fries, P. (2015). Rhythms for cognition: communication through coherence. Neuron *88*, 220–235.

Fries, P., Reynolds, J.H., Rorie, A.E., and Desimone, R. (2001). Modulation of oscillatory neuronal synchronization by selective visual attention. Science *291*, 1560–1563.

Golani, I., Benjamini, Y., and Eilam, D. (1993). Stopping behavior: constraints on exploration in rats (*Rattus norvegicus*). Behav. Brain Res. *53*, 21–33.

Herrmann, C.S., Munk, M.H., and Engel, A.K. (2004). Cognitive functions of gamma-band activity: memory match and utilization. Trends Cogn. Sci. *8*, 347–355.

Huerta, P.T., and Lisman, J.E. (1995). Bidirectional synaptic plasticity induced by a single burst during cholinergic theta oscillation in CA1 in vitro. Neuron *15*, 1053–1063.

Hyman, J.M., Wyble, B.P., Goyal, V., Rossi, C.A., and Hasselmo, M.E. (2003). Stimulation in hippocampal region CA1 in behaving rats yields long-term potentiation when delivered to the peak of theta and long-term depression when delivered to the trough. J. Neurosci. *23*, 11725–11731.

Igarashi, K.M., Lu, L., Colgin, L.L., Moser, M.B., and Moser, E.I. (2014). Coordination of entorhinal-hippocampal ensemble activity during associative learning. Nature *510*, 143–147.

Jarrard, L.E. (1993). On the role of the hippocampus in learning and memory in the rat. Behav. Neural Biol. *60*, 9–26.

Jensen, O., Kaiser, J., and Lachaux, J.P. (2007). Human gamma-frequency oscillations associated with attention and memory. Trends Neurosci. *30*, 317–324.

Jutras, M.J., Fries, P., and Buffalo, E.A. (2009). Gamma-band synchronization in the macaque hippocampus and memory formation. J. Neurosci. *29*, 12521–12531.

Jutras, M.J., Fries, P., and Buffalo, E.A. (2013). Oscillatory activity in the monkey hippocampus during visual exploration and memory formation. Proc. Natl. Acad. Sci. USA *110*, 13144–13149.

Kamiński, M.J., and Blinowska, K.J. (1991). A new method of the description of the information flow in the brain structures. Biol. Cybern. *65*, 203–210.

Kemere, C., Carr, M.F., Karlsson, M.P., and Frank, L.M. (2013). Rapid and continuous modulation of hippocampal network state during exploration of new places. PLoS ONE *8*, e73114.

Kesner, R.P., and Rolls, E.T. (2015). A computational theory of hippocampal function, and tests of the theory: new developments. Neurosci. Biobehav. Rev. *48*, 92–147.

Kesner, R.P., Lee, I., and Gilbert, P. (2004). A behavioral assessment of hippocampal function based on a subregional analysis. Rev. Neurosci. *15*, 333–351.

King, C., Recce, M., and O'Keefe, J. (1998). The rhythmicity of cells of the medial septum/diagonal band of Broca in the awake freely moving rat: relationships with behaviour and hippocampal theta. Eur. J. Neurosci. *10*, 464–477.

Knierim, J.J., Lee, I., and Hargreaves, E.L. (2006). Hippocampal place cells: parallel input streams, subregional processing, and implications for episodic memory. Hippocampus *16*, 755–764.

Komorowski, R.W., Manns, J.R., and Eichenbaum, H. (2009). Robust conjunctive item-place coding by hippocampal neurons parallels learning what happens where. J. Neurosci. *29*, 9918–9929.

MacKay, W.A., and Mendonça, A.J. (1995). Field potential oscillatory bursts in parietal cortex before and during reach. Brain Res. *704*, 167–174.

Malkova, L., and Mishkin, M. (2003). One-trial memory for object-place associations after separate lesions of hippocampus and posterior parahippocampal region in the monkey. J. Neurosci. *23*, 1956–1965.

Manns, J.R., and Eichenbaum, H. (2006). Evolution of declarative memory. Hippocampus *16*, 795–808.

Maris, E., and Oostenveld, R. (2007). Nonparametric statistical testing of EEG- and MEG-data. J. Neurosci. Methods *164*, 177–190.

McNaughton, N., Ruan, M., and Woodnorth, M.A. (2006). Restoring theta-like rhythmicity in rats restores initial learning in the Morris water maze. Hippocampus *16*, 1102–1110.

Mizuseki, K., Royer, S., Diba, K., and Buzsáki, G. (2012). Activity dynamics and behavioral correlates of CA3 and CA1 hippocampal pyramidal neurons. Hippocampus *22*, 1659–1680.

Montgomery, S.M., and Buzsáki, G. (2007). Gamma oscillations dynamically couple hippocampal CA3 and CA1 regions during memory task performance. Proc. Natl. Acad. Sci. USA *104*, 14495–14500.

Nicolelis, M.A., Baccala, L.A., Lin, R.C., and Chapin, J.K. (1995). Sensorimotor encoding by synchronous neural ensemble activity at multiple levels of the somatosensory system. Science *268*, 1353–1358.

Orr, G., Rao, G., Houston, F.P., McNaughton, B.L., and Barnes, C.A. (2001). Hippocampal synaptic plasticity is modulated by theta rhythm in the fascia dentata of adult and aged freely behaving rats. Hippocampus *11*, 647–654.

Rangel, L.M., Chiba, A.A., and Quinn, L.K. (2015). Theta and beta oscillatory dynamics in the dentate gyrus reveal a shift in network processing state during cue encounters. Front. Syst. Neurosci. *9*, 96.

Renner, M.J., and Seltzer, C.P. (1991). Molar characteristics of exploratory and investigatory behavior in the rat (*Rattus norvegicus*). J. Comp. Psychol. *105*, 326–339.

Save, E., Poucet, B., Foreman, N., and Buhot, M.C. (1992). Object exploration and reactions to spatial and nonspatial changes in hooded rats following damage to parietal cortex or hippocampal formation. Behav. Neurosci. *106*, 447–456.

Shirvalkar, P.R., Rapp, P.R., and Shapiro, M.L. (2010). Bidirectional changes to hippocampal theta-gamma comodulation predict memory for recent spatial episodes. Proc. Natl. Acad. Sci. USA *107*, 7054–7059.

Siegle, J.H., and Wilson, M.A. (2014). Enhancement of encoding and retrieval functions through theta phase-specific manipulation of hippocampus. eLife *3*, e03061.

Singer, W. (1999). Neuronal synchrony: a versatile code for the definition of relations? Neuron *24*, 49–65, 111–125.

Sławińska, U., and Kasicki, S. (1998). The frequency of rat's hippocampal theta rhythm is related to the speed of locomotion. Brain Res. *796*, 327–331.

Tallon-Baudry, C., Bertrand, O., Delpuech, C., and Permier, J. (1997). Oscillatory γ-band (30–70 Hz) activity induced by a visual search task in humans. J. Neurosci. *17*, 722–734.

Tiitinen, H., Sinkkonen, J., Reinikainen, K., Alho, K., Lavikainen, J., and Näätänen, R. (1993). Selective attention enhances the auditory 40-Hz transient response in humans. Nature *364*, 59–60.

Tort, A.B., Komorowski, R.W., Manns, J.R., Kopell, N.J., and Eichenbaum, H. (2009). Theta-gamma coupling increases during the learning of item-context associations. Proc. Natl. Acad. Sci. USA *106*, 20942–20947.

Trimper, J.B., Stefanescu, R.A., and Manns, J.R. (2014). Recognition memory and theta-gamma interactions in the hippocampus. Hippocampus *24*, 341–353.

Varela, F., Lachaux, J.P., Rodriguez, E., and Martinerie, J. (2001). The brainweb: phase synchronization and large-scale integration. Nat. Rev. Neurosci. *2*, 229–239.

Vinck, M., van Wingerden, M., Womelsdorf, T., Fries, P., and Pennartz, C.M. (2010). The pairwise phase consistency: a bias-free measure of rhythmic neuronal synchronization. Neuroimage *51*, 112–122.

Wang, Y., Romani, S., Lustig, B., Leonardo, A., and Pastalkova, E. (2015). Theta sequences are essential for internally generated hippocampal firing fields. Nat. Neurosci. *18*, 282–288.

Whishaw, I.Q., and Vanderwolf, C.H. (1973). Hippocampal EEG and behavior: changes in amplitude and frequency of RSA (theta rhythm) associated with spontaneous and learned movement patterns in rats and cats. Behav. Biol. *8*, 461–484.

Whishaw, I.Q., Gharbawie, O.A., Clark, B.J., and Lehmann, H. (2006). The exploratory behavior of rats in an open environment optimizes security. Behav. Brain Res. *171*, 230–239.

Winson, J. (1978). Loss of hippocampal theta rhythm results in spatial memory deficit in the rat. Science *201*, 160–163.

Witter, M.P., Wouterlood, F.G., Naber, P.A., and Van Haeften, T. (2000). Anatomical organization of the parahippocampal-hippocampal network. Ann. N Y Acad. Sci. *911*, 1–24.

Zarnadze, S., Bäuerle, P., Santos-Torres, J., Böhm, C., Schmitz, D., Geiger, J.R.P., Dugladze, T., and Gloveli, T. (2016). Cell-specific synaptic plasticity induced by network oscillations. eLife *5*, e14912.

Zheng, C., Bieri, K.W., Trettel, S.G., and Colgin, L.L. (2015). The relationship between gamma frequency and running speed differs for slow and fast gamma rhythms in freely behaving rats. Hippocampus *25*, 924–938.

Zheng, C., Bieri, K.W., Hwaun, E., and Colgin, L.L. (2016). Fast gamma rhythms in the hippocampus promote encoding of novel object-place pairings. eNeuro *3*, 1–19.

Cell Reports, Volume *21*

Supplemental Information

Gamma Oscillations in Rat Hippocampal Subregions

Dentate Gyrus, CA3, CA1, and Subiculum

Underlie Associative Memory Encoding

John B. Trimper, Claire R. Galloway, Andrew C. Jones, Kaavya Mandi, and Joseph R. Manns

Supplemental Tables

Table S1. Significant frequency clusters for Figure 2B and 2C[a]

Power	Region	Range	Cluster	Sum	97.5%	Shuffle Mean ± STD	p value (≤)	Effect[b] Size
	DG	3-12 Hz	6-12 Hz	4.91	1.92	0.11 ± 0.48	0.000	10.00
	DG	12-90 Hz	13-90 Hz	52.96	14.35	2.80 ± 4.76	0.000	10.54
	CA3	3-12 Hz	7-10 Hz	2.85	1.98	0.18 ± 0.63	0.009	4.24
	CA3	12-90 Hz	15-90 Hz	51.90	14.53	2.67 ± 4.36	0.000	11.29
	CA1	12-90 Hz	25-90 Hz	44.90	10.83	2.39 ± 3.71	0.000	11.46
	SUB	3-12 Hz	6-10 Hz	3.92	1.93	0.15 ± 0.55	0.000	6.85
	SUB	12-90 Hz	45-89 Hz	30.72	11.52	2.60 ± 3.60	0.000	7.81
	Average	3-12 Hz	6-12 Hz	4.85	0.00	0.00 ± 0.06	0.000	80.8
	Interaction	3-12 Hz	7-10 Hz	2.98	2.00	0.08 ± 0.41	0.000	7.07
	Interaction	12-90 Hz	13-90 Hz	53.00	0.00	0.02 ± 0.28	0.000	189.2
Coherence	Regions	Range	Cluster	Sum	97.5%	Shuffle Mean ± STD	p value (≤)	Effect Size
	DG/CA3	12-90 Hz	13-89 Hz	52.82	11.33	2.46 ± 3.74	0.000	13.47
	CA3/CA1	3-12 Hz	7-9 Hz	1.99	1.93	0.09 ± 0.42	0.005	4.52
	CA3/CA1	12-90 Hz	32-50 Hz	12.50	10.76	2.35 ± 3.40	0.016	2.99
	CA1/SUB	3-12 Hz	7-12 Hz	3.96	2.86	0.20 ± 0.67	0.002	5.61
	CA1/SUB	12-90 Hz	13-26 Hz	9.90	8.81	2.14 ± 3.19	0.016	2.43
	Interaction	3-12 Hz	6-12 Hz	5.00	2.75	0.18 ± 0.64	0.000	7.53
	Interaction	12-90 Hz	13-63 Hz	34.84	26.97	3.44 ± 8.07	0.000	3.89

a. Data were evaluated separately for 3-12 Hz vs. 12-90 Hz ranges, and thus a 97.5 percentile criterion was used to evaluate statistical significance of observed cluster sums.
b. Effect size was calculated as a z score of the cluster sum in relation to the average and standard deviation of the shuffle distribution.

Table S2. Significant time clusters for Figure 3B and 3C[a]

Slow Gamma Power	Region	Cluster (s)	Sum	95%	Shuffle Mean ± STD	p value (≤)	Effect[b] Size
	DG	-0.45 to 0.00	9.64	8.69	2.75 ± 3.48	0.036	1.98
	DG	0.30 to 1.80	29.53	8.69	2.75 ± 3.48	0.000	7.70
	CA3	-0.75 to 0.00	15.45	8.61	2.42 ± 3.23	0.002	4.03
	CA3	0.30 to 1.80	29.05	8.61	2.42 ± 3.23	0.000	8.24
	CA1	0.50 to 1.10	11.45	8.59	2.43 ± 3.35	0.018	2.69
Slow Gamma Coherence	**Regions**	**Cluster (s)**	**Sum**	**95%**	**Shuffle Mean ± STD**	**p value (≤)**	**Effect Size**
	DG/CA3	0.60 to 1.80	23.24	8.61	2.40 ± 3.21	0.000	6.49
	CA3/CA1	0.40 to 1.20	15.16	8.32	2.46 ± 3.20	0.003	3.97
	CA3/CA1	1.30 to 1.80	9.49	8.32	2.46 ± 3.20	0.030	2.20
Fast Gamma Power	**Region**	**Cluster (s)**	**Sum**	**95%**	**Shuffle Mean ± STD**	**p value (≤)**	**Effect Size**
	DG	-0.049 to 1.80	36.34	9.34	2.56 ± 3.53	0.000	9.57
	CA3	-0.15 to 1.80	38.60	8.36	2.18 ± 3.20	0.000	11.38
	CA1	-0.049 to 1.30	26.77	8.57	2.13 ± 3.11	0.000	7.92
	SUB	-0.40 to 0.15	11.63	8.92	2.92 ± 3.52	0.017	2.47
	SUB	0.65 to 1.80	22.59	8.92	2.92 ± 3.52	0.001	5.59
Fast Gamma Coherence	**Regions**	**Cluster (s)**	**Sum**	**95%**	**Shuffle Mean ± STD**	**p value (≤)**	**Effect Size**
	CA3/CA1	0.25 to 0.90	13.72	7.73	2.40 ± 3.00	0.002	3.77

a. A 95 percentile criterion was used to evaluate statistical significance of observed cluster sums.
b. Effect size was calculated as a z score of the cluster sum in relation to the average and standard deviation of the shuffle distribution.

Table S3. Percent of Neurons Significantly Phase Modulated by Range and Subregion/Subregion Pair in Figure 4 and Figure S4

Neurons Modulated by Local Field (Related to Figure 4)				
	Theta	Beta	Slow Gamma	Fast Gamma
DG/DG[a]	79% (54/68)[b]	48% (30/62)	57% (33/58)	28% (16/57)
CA3/CA3	40% (72/180)	26% (57/216)	27% (58/213)	38% (81/215)
CA1/CA1	51% (142/280)	29% (88/308)	13% (38/289)	15% (45/300)
SUB/SUB	67% (29/43)	36% (16/45)	22% (10/46)	32% (14/44)

Neurons Modulated by Downstream Field (Related to Figure S4)				
	Theta	Beta	Slow Gamma	Fast Gamma
DG/CA3	64% (38/59)	67% (39/58)	70% (37/53)	60% (33/55)
CA3/CA1	52% (95/184)	22% (43/193)	18% (34/187	23% (42/183)
CA1/SUB	79% (262/333)	23% (74/328)	9% (29/307)	10% (31/296)

a. The first subregion in the pair indicates which subregion's spikes were being considered while the second subregion listed indicates the subregion from which the local field potential was drawn. E.g., "CA3/CA1" indicates CA3 spiking was being compared to oscillations recorded from CA1.

b. Values are presented as the percent of total neurons recorded that were significantly modulated by oscillatory phase. The raw number of significantly modulated neurons and the total number of neurons recorded are in parentheses.

Table S4. Significant frequency clusters for Figure 6A[a]

Power	Region	Range	Cluster	Sum	97.5%	Shuffle Mean ± STD	p value (≤)	Effect[c] Size
	DG	12-90 Hz	26-59 Hz	22.72	10.43	2.28 ± 3.27	0.000	6.25
	CA3	12-90 Hz	25-51 Hz	18.56	10.74	2.32 ± 3.43	0.002	4.73
	Average	12-90 Hz	25-59 Hz	23.47	0[b]	0 ± 0	0.000	Inf[d]
	Interaction	12-90 Hz	32-50 Hz	12.75	5.50	0.34 ± 2.17	0.000	5.72

a. Data were evaluated separately for 3-12 Hz vs. 12-90 Hz ranges, and thus a 97.5 percentile criterion was used to evaluate statistical significance of observed cluster sums.

b. A value of 0 for the 97.5% criterion indicates that no randomly-generated clusters surpassed the initial cluster threshold (see Experimental Procedures for details)

c. Effect size was calculated as a z score of the cluster sum in relation to the average and standard deviation of the shuffle distribution.

d. A value of infinity is possible when no randomly-generated clusters surpassed the initial cluster threshold, and therefore the average and standard deviation for the shuffle distribution are equal to zero.

Table S5. Statistics for Bar Graphs in Figure 6C (Power), 6D (Coherence), and 6E (DTF)

		One-Way RM ANOVA			Linear Trend		
Slow Gamma		F (2,10)	p	partial η^2	F (1,5)	p	partial η^2
	Power						
	DG	14.353	0.001	0.742	28.458	0.003	0.851
	CA3	12.935	0.002	0.721	16.794	0.009	0.771
	CA1	2.177	0.164	0.303	2.497	0.175	0.333
	SUB	0.829	0.464	0.142	4.193	0.096	0.456
	Average	11.662	0.002	0.700	15.583	0.011	0.757
	Coherence						
	DG/CA3	0.995	0.404	0.166	2.251	0.194	0.310
	CA3/CA1	0.666	0.535	0.118	0.007	0.983	0.001
	CA1/SUB	3.393	0.075	0.404	6.994	0.046	0.583
	Average	2.842	0.105	0.362	11.851	0.018	0.703
	DTF						
	DG/CA3	4.145	0.049	0.453	8.010	0.037	0.616
	CA3/CA1	2.170	0.165	0.303	2.274	0.192	0.313
	CA1/SUB	0.390	0.687	0.072	0.622	0.466	0.111
	Average	9.088	0.006	0.645	19.348	0.007	0.795
Fast Gamma		F (2,10)	p	partial η^2	F (1,5)	p	partial η^2
	Power						
	DG	4.012	0.053	0.445	4.775	0.081	0.489
	CA3	3.186	0.085	0.389	3.595	0.116	0.418
	CA1	1.184	0.345	0.192	1.086	0.345	0.178
	SUB	0.340	0.720	0.064	0.293	0.611	0.055
	Average	1.983	0.188	0.284	2.010	0.215	0.287
	Coherence						
	DG/CA3	0.278	0.763	0.053	0.079	0.790	0.016
	CA3/CA1	0.098	0.908	0.19	0.097	0.769	0.019
	CA1/SUB	0.110	0.897	0.021	0.035	0.858	0.007
	Average	0.053	0.949	0.010	0.068	0.804	0.013
	DTF						
	DG/CA3	0.849	0.456	0.145	0.538	0.496	0.097
	CA3/CA1	0.607	0.564	0.108	0.627	0.464	0.111
	CA1/SUB	0.631	0.552	0.112	0.752	0.426	0.131
	Average	0.406	0.677	0.075	0.003	0.959	0.001

Table S6. Significant frequency clusters for Figure 7A and 7B[a]

Power	Region	Range	Cluster	Sum	97.5%	Shuffle Mean ± STD	p value (≤)	Effect[c] Size
	Average	12-90 Hz	28-40 Hz	8.66	0[b]	0.00 ± 0.00	0.000	Inf[d]
	Interaction	12-90 Hz	67-75 Hz	5.65	0[b]	0.01 ± 0.22	0.000	25.64
Coherence	Regions	Range	Cluster	Sum	97.5%	Shuffle Mean ± STD	p value (≤)	Effect Size
	CA1/SUB	12-90 Hz	26-41 Hz	10.27	8.74	1.92 ± 2.84	0.010	2.94

a. Data were evaluated separately for 3-12 Hz vs. 12-90 Hz ranges, and thus a 97.5 percentile criterion was used to evaluate statistical significance of observed cluster sums.
b. A value of 0 for the 97.5% criterion indicates that no randomly-generated clusters surpassed the initial cluster threshold of (see Experimental Procedures for details).
c. Effect size was calculated as a z score of the cluster sum in relation to the average and standard deviation of the shuffle distribution.
d. A value of infinity is possible when no randomly-generated clusters surpassed the initial cluster threshold, and therefore the average and standard deviation for the shuffle distribution are equal to zero.

Table S7. Statistics for Bar Graphs in Figure 7C (Power), 7D (Coherence), and 7E (DTF)

		One-Way RM ANOVA			Linear Trend		
Slow Gamma		F (2,10)	p	partial η^2	F (1,5)	p	partial η^2
	Power						
	DG	4.521	0.040	0.475	11.639	0.019	0.699
	CA3	3.725	0.062	0.427	6.835	0.047	0.578
	CA1	1.581	0.253	0.240	1.651	0.255	0.248
	SUB	1.025	0.394	0.170	3.858	0.107	0.436
	Average	3.504	0.070	0.412	6.835	0.047	0.578
	Coherence						
	DG/CA3	5.138	0.029	0.507	40.294	0.001	0.890
	CA3/CA1	0.348	0.715	0.065	0.398	0.556	0.074
	CA1/SUB	4.611	0.038	0.480	5.672	0.063	0.531
	Average	5.330	0.027	0.516	14.410	0.013	0.742
	DTF						
	DG/CA3	1.869	0.204	0.272	3.038	0.142	0.378
	CA3/CA1	0.438	0.657	0.080	0.061	0.815	0.12
	CA1/SUB	0.812	0.471	0.140	0.610	0.470	0.109
	Average	1.759	0.222	0.260	2.709	0.161	0.351
Fast Gamma		F (2,10)	p	partial η^2	F (1,5)	p	partial η^2
	Power						
	DG	2.970	0.097	0.373	0.437	0.538	0.080
	CA3	1.045	0.387	0.173	1.281	0.309	0.204
	CA1	1.821	0.212	0.267	1.870	0.280	0.272
	SUB	1.285	0.319	0.204	1.265	0.312	0.202
	Average	1.043	0.388	0.173	0.337	0.587	0.063
	Coherence						
	DG/CA3	0.931	0.426	0.157	0.236	0.647	0.045
	CA3/CA1	3.894	0.056	0.438	15.981	0.010	0.762
	CA1/SUB	1.109	0.369	0.181	0.783	0.417	0.135
	Average	1.548	0.260	0.236	0.984	0.367	0.164
	DTF						
	DG/CA3	0.190	0.830	0.037	0.013	0.915	0.002
	CA3/CA1	0.321	0.733	0.060	0.012	0.917	0.002
	CA1/SUB	1.274	0.321	0.203	0.628	0.464	0.112
	Average	0.189	0.830	0.036	0.016	0.904	0.003

Supplemental Figures and Legends

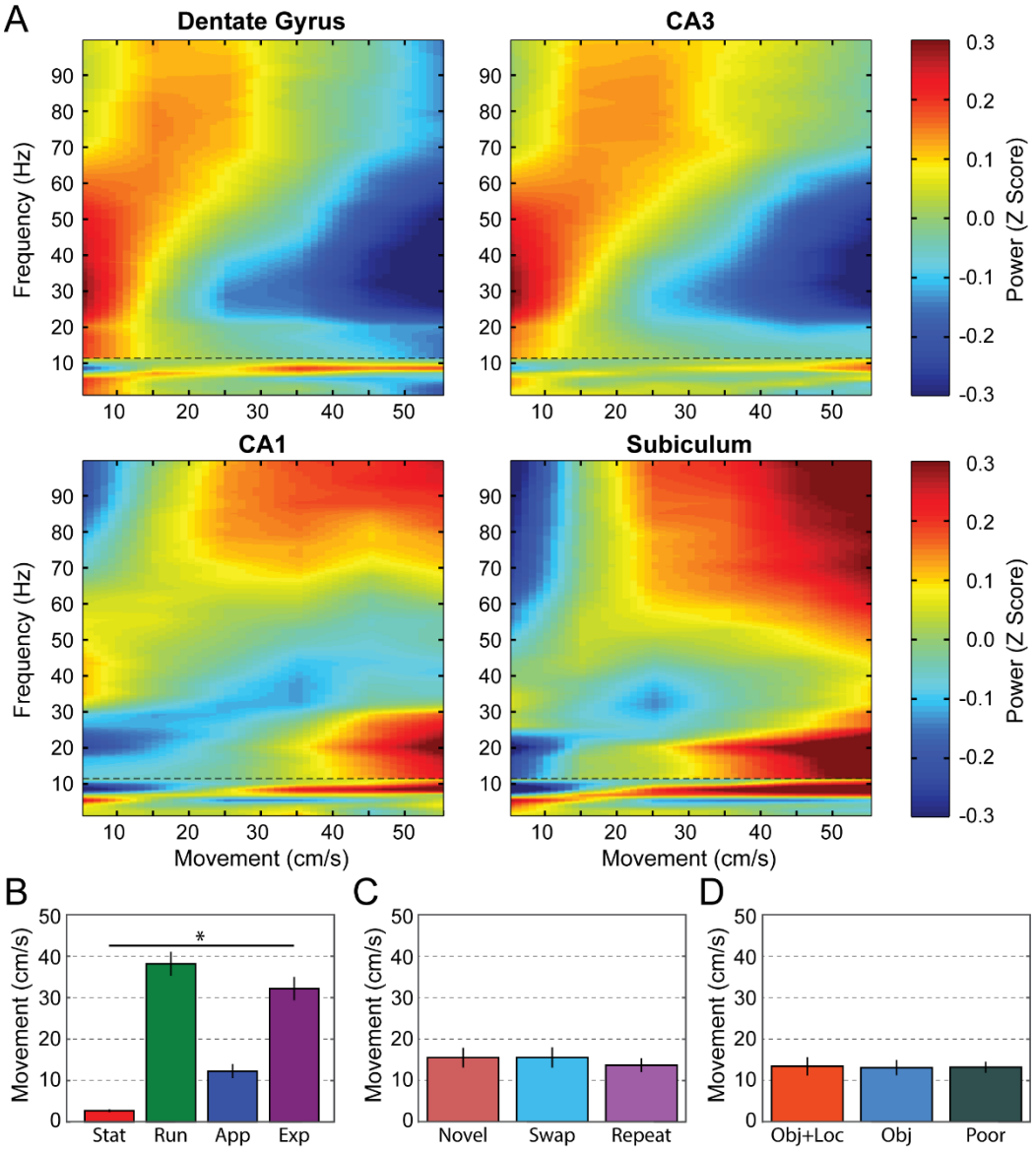

Figure S1, Related to Figure 2. (A). Spectral power differed by subregion and speed of locomotion. Power is shown for each subregion across a broad range of frequencies (1-100 Hz) and speeds of movement (5-55 cm/s). Power is z scored across speed bins within each frequency bin. A dotted line at 12 Hz is shown to indicate that separate taper parameters were employed for >= 12 Hz and for <= 12 Hz. The results for CA3 and CA1 were similar to those presented previously (Ahmed & Mehta, 2012; Kemere et al., 2013; Zheng et al., 2015). Apparent here is the strong degree of similarity between DG and CA3, and between CA1 and subiculum with regards to variation in spectral power by speed of locomotion. **(B).** Average speed of movement was significantly different ($p<0.001$) across behavioral states (S = Stationary; R = Run; E = Exploration; A = Approach). **(C).** Average speed of movement during exploration of objects on lap 3 did not statistically significantly ($p. > .05$) differ by object condition. Speed of movement was averaged across the neural analysis window. **(D)**. Average speed of movement during exploration of novel objects on lap 1 did not statistically significantly ($p. > .05$) differ by memory condition. Speed of movement was averaged across the neural analysis window. Error bars show SEM throughout the figure.

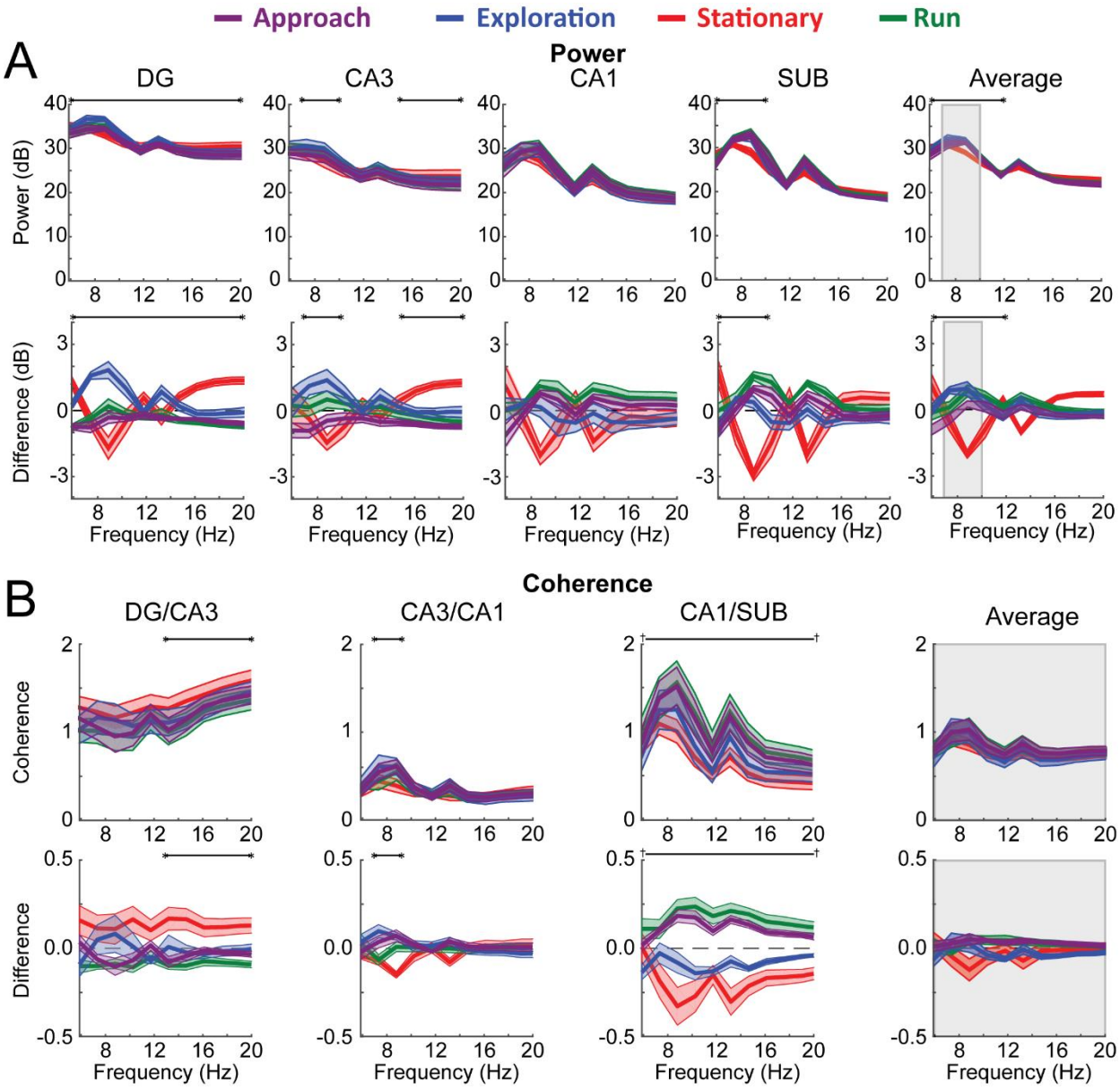

Figure S2, Related to Figure 2. Each subplot presents data identical to that presented in Figure 2, but expanded from 6-20 Hz to visually emphasize differences present in this lower frequency range. (A) Spectral power from 6-20 Hz is shown across the four behavioral states under consideration [i.e., Approach (Purple), Exploration (Blue), Stationary (Red), and Run (Green)]. Frequency clusters that differ significantly across the four behavioral states within each subregion, and with regards to power averaged across subregions, are indicated by bars above each panel bookended by asterisks. Statistical details for each cluster can be seen in Table S1. A significant interaction across behavioral states and subregions is indicated by the gray box presented over the Average hippocampal power subplot (far right). All significant differences presented in this panel, indicated with black lines bookended by asterisks, withstood a Bonferonni alpha correction of 0.05/5, with the denominator chosen based on the number of subregions analyzed plus one for the average across subregions. (B) Coherence from 6-20 Hz is shown for each pair of directly connected subregions, as well as for the average across subregion pairs. Significant differences are indicated as in A, however, here, significant differences are also present that did not withstand a Bonferonni alpha correction of 0.05/4 (for 3 subregion pairs plus the average across pairs). These differences are indicated by black

lines bookended by the dagger symbol (†).

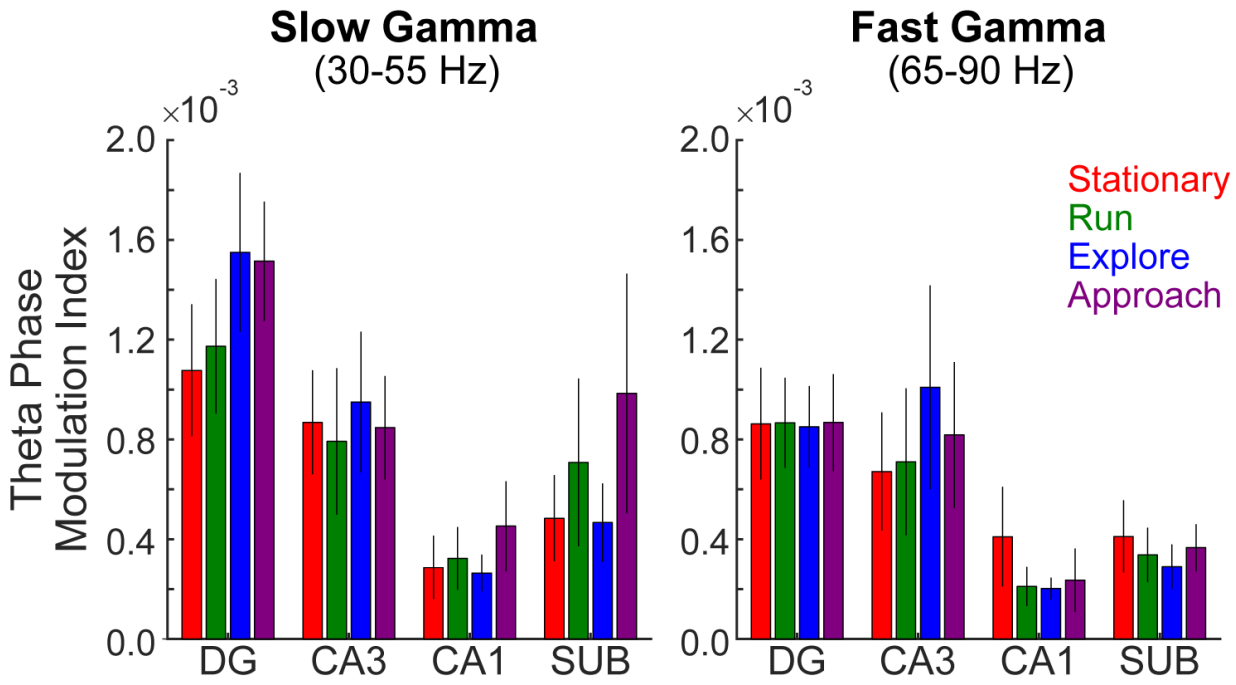

Figure S3. Related to Figure 2. Mean theta-phase modulation index of slow gamma (left panel) and fast gamma (right panel) amplitude. The data are shown for each behavioral state (stationary, run, explore, and approach) for each hippocampal region. Modulation indices were similar across behavioral states (see text). Error bars reflect standard error of the mean across rats (n=6).

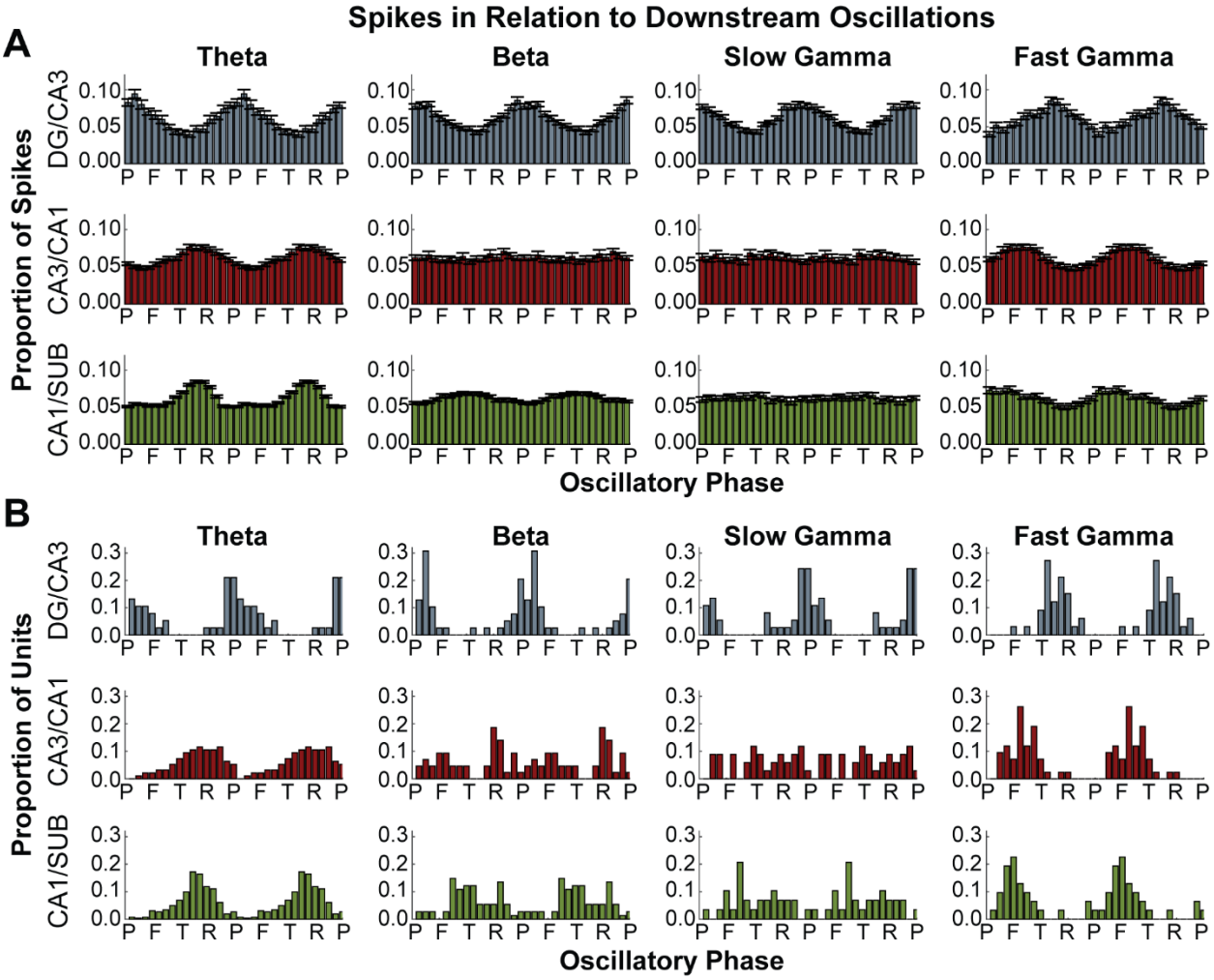

Figure S4, Related to Figure 4. (A) Plotted are the average distributions of action potentials in each subregion relative to the phase (P = peak; F = falling; T = trough; R = rising) of distinct oscillatory rhythms (denoted at top) recorded from the downstream subregion (e.g., the DG/CA3 plot for theta refers to DG spikes in relation to CA3 theta). Averages and error (SEM) are across all neurons found to be significantly phase modulated ($p < 0.05$, Rayleigh's Test). See Table S3 for the percent of neurons by subregion found to be significantly phase modulated. Spiking in relation to each rhythm was only considered when that rhythm was strong (see Methods) and therefore, these graphs do not necessarily represent the same action potentials, nor the same sample of neurons. The finding that many neurons from each subregion aligned their spiking to these rhythms implies that spikes from upstream regions are able to impact oscillatory activity downstream. Note that the data is plotted twice, replicated across the oscillatory cycle, to aid visualization of periodicity. **(B)** Shown are the distributions across significantly phase modulated neurons of average preferred oscillatory phase for spiking. Note the consistency of preferred phase for neurons in some subregions in relation to distinct rhythms (e.g., subicular neurons and spikes in relation to theta) relative to the lack of a consistent phase preference for other subregions (e.g., CA1 spikes to SUB slow gamma oscillations). As with B, all data is plotted twice across the x axis for visualizing periodicity.

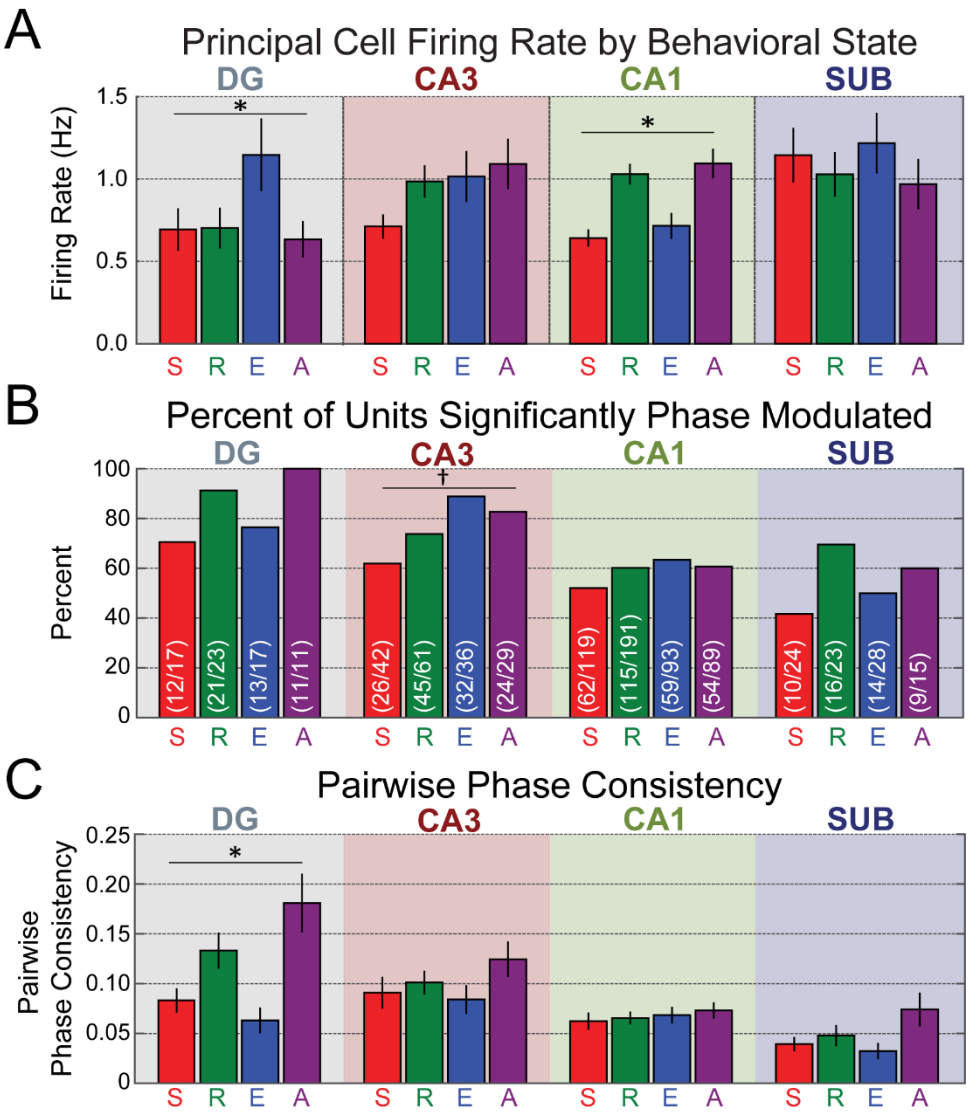

Figure S5. Related to Figure 4. (A) Average firing rate by subregion for each behavioral state (S = Stationary; R = Run; E = Exploration; A = Approach). Error bars reflect standard error of the mean across neurons. After alpha correction, firing rate differed significantly only for CA1 ($p = <0.0001$), reflected by firing rates most elevated during locomotive states (Approach and Run) relative to non-locomotive states (Exploration and Stationary), and DG ($p = 0.006$) whose firing rate was greatest during object exploration. **(B).** Principal cell firing aligned strongly with theta recorded from CA1. Bars reflect the percent of significantly phase modulated neurons out of total number of neurons for each behavioral state (S = Stationary; R = Run; E = Exploration; A = Approach) and each subregion DG, CA3, CA1, and SUB (subiculum)]. The percent of neurons did not differ significantly for any region after Bonferonni alpha correction for four subregions (DG: $p = 0.114$; CA3: $p = 0.035$; CA1: $p = 0.345$; SUB, $p = 0.250$). Percentages reflected by all bars presented were significantly greater than chance (~5%) as tested with a random permutation approach in which the actual percent of neurons statistically modulated by phase were compared to the percentages attained from 1000 shuffles where the number of spikes and neurons remains constant, but spike phases were randomly drawn from a circular uniform distribution. **(C)** Pairwise Phase Consistency for the neurons recorded from each subregion divided by behavioral state. In DG, pairwise phase consistency differed significantly across conditions such that the most elevated levels were observed for locomotive relative to non-locomotive states ($p < 0.001$). More detailed statistics are presented the Results and Discussion section.

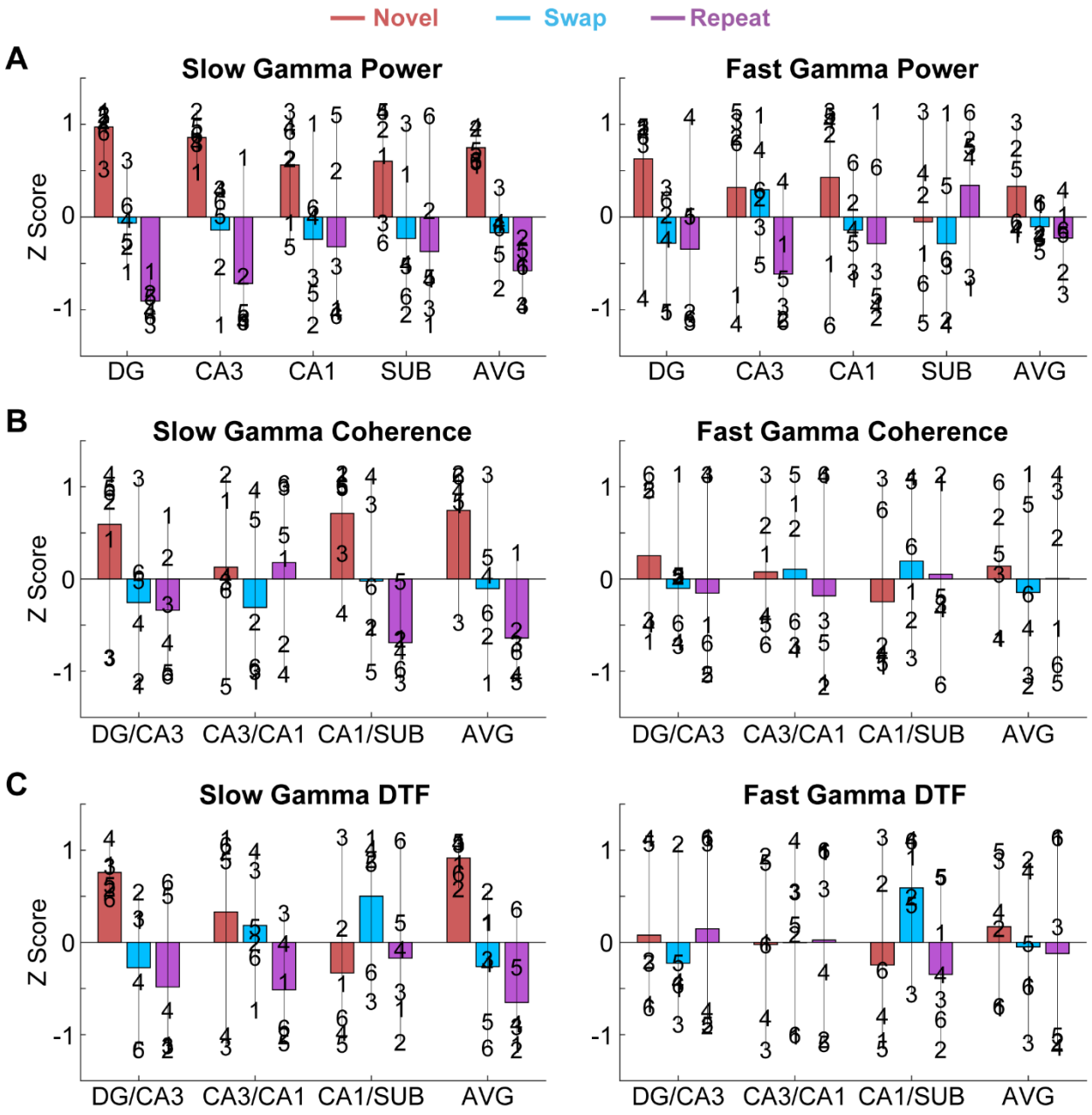

Figure S6, Related to Figure 6. The data from Figure 6, showing spectral measures during the first 1 s of object exploration on lap 3 split by object condition, is reproduced here but with each rat's data represented by an identifying number for better visualization of variability across rats. Data was z-scored to account for magnitude differences with increasing frequency due to spectral power exhibiting a 1/f distribution, and for improved visualization of effect magnitude. (A) Z scored slow gamma and fast gamma power for each subregion and for the average across subregions. (B) Z scored slow gamma and fast gamma coherence between each pair of directly connected subregions and averaged across subregion pairs. (C) Z scored slow gamma and fast gamma directed transfer function (DTF). For statistical information, see significance markers in Figure 6 and statistical details presented in Table S5.

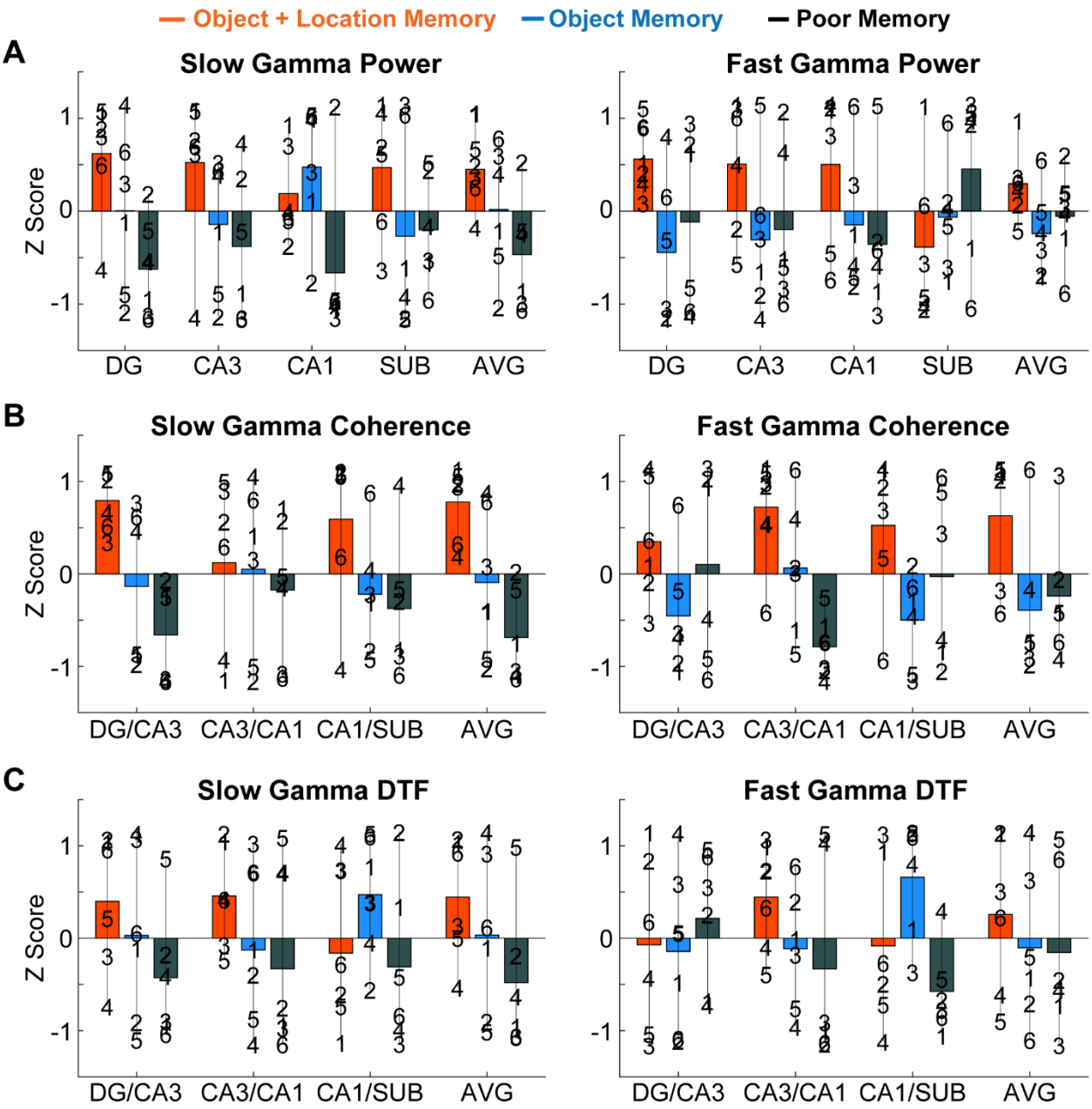

Figure S7, Related to Figure 7. The data from Figure 7, showing spectral measures during the first 1.5 s of object exploration on lap 1 split by subsequent memory, is reproduced here but with each rat's data represented by an identifying number for better visualization of variability across rats. (A) Z scored slow gamma and fast gamma power for each subregion and for the average across subregions. (B) Z scored slow gamma and fast gamma coherence between each pair of directly connected subregions and averaged across subregion pairs. (C) Z scored slow gamma and fast gamma directed transfer function (DTF). For statistical information, see significance markers in Figure 7 and statistical details presented in Table S7.

Supplemental Experimental Procedures

Behavioral Training

The behavioral task required rats to run consecutive clockwise laps around an elevated circular track (diameter = 91.5cm/ track width = 7 cm) for small chocolate sprinkle rewards at the completion of each lap. Rats were trained daily to perform these laps up to criteria (80 laps in 40 minutes), a process lasting approximately five weeks. Throughout the training process, rats were additionally habituated to touching of their heads in anticipation of the neural recording experiments. After surgical implantation of a chronic neural recording assembly (see below), rats were re-trained daily up to criteria, at which point performance was maintained with approximately twice-weekly training sessions until recording tetrodes were in position. One day before initial testing, rats were exposed to objects placed on retractable flaps adhered to the perimeter of the elevated track for the purpose of reducing potential neophobia at test related to rats never having encountered any objects before along the track.

During recognition memory testing (see Figure 5 and main text), the degree of exploration of objects was at the rats' discretion, relying on rats' innate curiosity and preference for novelty, and never rewarded, encouraged, or otherwise manipulated by experimenters. When objects were repeated from a prior lap, duplicates were employed to avoid scent marking. The memory conditions assigned to each trial alternated in a 2:1 fashion, such that there were two Swap trials for every one Repeat/Novel trial. The locations for the Repeat and Novel objects were counter-balanced across trials. The number of trials and test sessions conducted in any single day was limited by the quality of recordings and rat performance (i.e., willingness to explore objects at study on lap 1).

Objects

Example objects can be seen in Figure 5. Objects were randomly pulled from a set of approximately 320 unique objects, with up to four duplicates of each unique object. All objects were purchased from a local store to be used solely for object recognition memory testing with rats in our laboratory. Objects ranged in size from approximately 7 x 7 x 7 cm to 17 x 17 x 10 cm. Object size was equated within trials to control for exploration time effects related to this factor. Objects were randomly assigned to experimental conditions. All objects were novel to rats at the beginning of testing, and were washed immediately after testing, with all duplicates of that object, to limit scent marking and ensure all duplicates of the same objects were handled similarly. Objects were adhered to retractable flaps on the outside of the elevated circular track using Velcro.

Surgical Procedure

Sterile-tip stereotaxic surgery was performed after rats were deeply anesthetized with isoflurane (1–3% in oxygen) and given buprenorphine (0.05 mg/kg) as an analgesic. Rats were implanted with a custom chronic electrophysiological recording headstage that contained up to 32 independently movable tetrodes. Tetrodes were funneled through two stainless steel cannulae (14 gauge and 17 gauge) to concentrate their positioning over the hippocampal subregions of interest—DG, CA3, CA1, and subiculum. Craniotomies spanned an area from approximately 2.6 to 6.4 mm posterior to bregma and 1.3 to 4.2 mm lateral to the central suture, with tetrodes typically falling within 3 to 6 mm posterior to bregma and 1.8 to 3.8 mm lateral to the central suture. Each tetrode consisted of four 12.5 μm nichrome wires whose tips were plated with gold to reduce the impedance to 200 kΩ at 1 kHz. Rats were monitored in the lab for several hours after surgery, and daily for the following three days. Additional doses of buprenorphine (0.05 mg/kg) were given immediately after surgery and the following morning. Meloxicam (Metacam) was administered immediately after surgery (0.75ml) and each of the two following mornings for pain relief.

Neural Data Acquisition

Following a one-week recovery period, tetrodes were gradually lowered over the course of 1-3 months to the pyramidal layers of CA3, CA1, and subiculum and the granule cell layer of DG occurred over several weeks and was assisted by known electrophysiological hallmarks [e.g., dentate spikes (Bragin et al., 1995), sharp-wave ripples (Buzsaki., 1986)]. A stainless steel screw implanted in the skull above the cerebellum served as the reference for LFPs during recording, whereas a tetrode within the hippocampus but without single units served as the reference for spike channels. Neural data were acquired using NSpike data acquisition system (nspike.sourceforge.net). Tetrodes were never turned prior to testing on days in which experiments were performed, though minor adjustments were made after test sessions to maintain good single unit isolation for the following days.

For LFP analyses in CA3, CA1, and subiculum, one tetrode in the middle third of each region's transverse axis (proximal to distal relative to DG) was selected for each rat. This intermediate portion along the proximal/distal axis was selected because the intermediate portion of CA3 projects directly to the intermediate portion in CA1 which projects to the intermediate portion of subiculum, and because this portion of each of the regions receives input from both lateral and medial entorhinal cortex (Witter and Amaral, 2004). The intermediate portion of DG was not selectively targeted as dentate cells project to the entire transverse extent of CA3 (Swanson et al., 1978; Gaarskjaer, 1986).

Statistical Reporting Format

Unless otherwise noted, all figures and central tendency reporting is provided as mean plus and minus the standard error of the mean.

Behavioral Coding.

Experimental videos were scored using custom written software. A behavioral flag was assigned to each event of interest (e.g., lap start and end times, object exploration initiation and offset). Rats were considered to be exploring objects only when their noses were within approximately 1 cm of the object and rats were exhibiting signs of active investigation. Exploration events including excessive chewing were discarded and data for that trial were not used. For analyses of rat locomotion, rats' positions were tracked within the videos in Cartesian coordinates using custom written software in MATLAB (Mathworks) which detected the centroid of two LEDs affixed to the recording headstage on rats' heads. The frame rate of the video was 30 frames per second.

We separated rats' activity on blank laps into periods of time in which the rat was not locomoting (Stationary) and periods of time in which the rats were locomoting (Run). To accomplish this task, spatial coordinate data (see above) and LFP data on blank laps were divided into 250 ms segments. Stationary bouts were defined as 8 consecutive 250 ms segments in which rats moved less than 10 cm/s. Run bouts were defined as 8 consecutive 250 ms segments in which rats moved more than 10 cm/s. A threshold of 10 cm/s, rather than 0 cm/s, was chosen to allow for small head movements and rearing in the Stationary condition. Exploration bouts were defined as period of time lasting at least 2 s in which rats were consistently engaging in active investigation of novel objects, while Approach bouts were defined as the 2s of time immediately preceding exploration onset.

Analyses of Neural Data.

Power and Coherence. All data analyses were performed using custom written code in MATLAB (Mathworks). Spectral analyses implemented a multitaper fast Fourier transform method for calculating coherence and power (Bokil et al., 2010). Spectral power, also referred to as spectrum or auto-spectra, is a metric providing information about the prevalence of oscillatory activity at each frequency within a LFP sweep. Power was calculated as the product of the complex Fourier coefficients multiplied by their complex conjugate. Power was log-transformed to account for a 1/frequency distribution, and converted from bels to decibels by multiplying log transformed values by ten. Coherence is a metric for covariance of phase and amplitude between two LFPs. It was calculated as the absolute magnitude of coherency, which is cross spectrum normalized by the product of the two auto-spectra (i.e., power for each LFP). Coherence was Fisher transformed to stabilize variance at the tails of the distribution, thus explaining why values greater than 1 were observed when coherence was particularly high. Unless noted otherwise, sliding 0.5 s windows with step size of 0.05 s were used to calculate spectral estimates to reduce the possible complication of nonstationarity in the data (Mitra and Pesaran, 1999). To ensure adequate spectral resolution within each frequency range of interest, multitaper FFTs employed separate taper parameters for the theta range and below (1 – 13 Hz) relative to 13 Hz and above (13 – 90 Hz). For 1 – 13 Hz, we used a frequency half bandwidth of 1 Hz (-1 Hz to +1 Hz) and a single taper for each 0.5 s section of data. For 13 Hz and above, we used a frequency half bandwidth of 6 Hz (-6 Hz to +6 Hz), enabling the use of five well-concentrated orthogonal tapers for each 0.5 s section of data. To account for possible bias in spectral metric calculation, in cases where an uneven number of trials were present across conditions within a rat, a subsampling procedure where trials for each condition were subsampled down to the lowest number of trials present across conditions was performed. Subsampling was repeated 1,000 times, or the max allowable number of times when the max number of unique subsamples was less than 1,000. The final values for each condition were then calculated by averaging across these subsampling iterations.

Directed Transfer Function. Non-normalized directed transfer function, also referred to as the transfer matrix (H), is the inverse of the fast Fourier transformed multivariate autoregressive coefficient matrix. Non-normalized directed transfer function is an autoregressive metric that assesses the ability of the past history of time series X, back to a specified lag (model order), to predict the current state of time series Y (Kaminski & Blinowska, 1991). Non-normalized directed transfer function can be considered a form of multivariate Granger causality in the frequency domain. Units are arbitrary. Prior to calculation, LFP amplitudes were z scored within subregion to equate amplitude variability across subregions. As with the multitaper approach described above, different parameter sets were employed for 13 Hz and below relative to greater than 13 Hz to improve spectral and temporal resolution. For 5-13 Hz, LFP traces were downsampled by a factor of 14, adjusting the sampling rate to 107.14 Hz. This downsampling factor was chosen as the highest number possible that would still prevent aliasing, allowing for at least eight data points per cycle in the highest frequency under consideration within this range of interest (5 – 13 Hz) [e.g., with 1500 Hz sampling rate, requiring 8 data points per cycle from a 13 Hz oscillation requires at least 1500 Hz / (13 Hz * 8 points) data points (107.14) per second]. A model order of 20 was chosen to accompany at least 1

complete cycle of a 6 Hz theta oscillation. For the higher frequency range, from 14-90 Hz, data was downsampled by a factor of 2 adjusting the sampling rate to 750 Hz allowing for at least 8 data points per cycle of a 90 Hz oscillation. A model order of 30 was chosen, allowing for at least one complete cycle of a 25 Hz oscillation within the specified lag. Model parameters were validated a priori on a subset of the data by verifying whiteness of the noise coefficients, weak correlation among the residuals, stability/stationarity of the model, and consistency of the model. Model validation was performed using the SIFT toolbox (Delorme et al., 2011; Mullen, 2014), implemented through EEGlab (Delorme & Makeig, 2004), and following the suggestions of Ding et al., 2000.

Statistical testing of frequency clusters. A cluster-based permutation approach adapted from (Maris et al., 2007; Maris & Oostenveld, 2007) for more than a single independent variable and more than two levels of each variable was employed. A description of the procedure is as follows. For each frequency bin, an F ratio was calculated. For questions regarding interactions between subregion/subregion pairing and condition, the F ratio was calculated with a two-way repeated measures analysis of variance (ANOVA) with subregion/subregion pairing as one factor and object condition as a second factor. For questions regarding an effect of condition *within* subregion/subregion pairing, a one-way ANOVA was employed with condition as the sole factor. This procedure produced a vector of F values spanning all frequency bins under consideration. To identify potentially-significant frequency clusters, F ratios were next converted to p values corresponding to the lower tail of the F distribution. Thus, higher p values here indicated a lower statistical probability of occurrence (so as to facilitate the cluster-summing procedure described below). This procedure produced a vector of p values spanning all frequency bins under consideration. All p values greater than 0.90 (upper 10^{th} percentile) were then identified as potential clusters and only consecutive groups of those p values of at least a pre-defined length were further considered (two consecutive points for below 13 Hz, four consecutive points for above 13 Hz). The choice of initial cluster detection threshold ($p = 0.90$) is arbitrary but is necessary to identify potential clusters. Separate cluster length criteria were used for the lower and higher frequency ranges as number of frequency bins differed greatly between the two ranges, with far less available in the low frequency range (<= 13 Hz). P values within each identified cluster of points were summed, such that a single sum was recorded for each cluster of sufficient length. These cluster sums recorded from the nonrandomized data were then compared to the maximum cluster sums recorded from each of 1,000 randomizations. This comparison against a random distribution essentially asks: is the difference across conditions present within this particular frequency range greater than the difference that might be observed by chance? When looking for significant differences across conditions within a subregion/subregion pairing, conditions were randomized within rats. When looking for significant interactions between subregion/subregion pairing and condition, both subregion/subregion pairing and condition were randomized within rats. Just as with the non-randomized data, cluster sums were identified in the averages across rats. Cluster sums from the non-randomized data greater than the 97.5^{th} percentile for the randomized cluster sums were denoted as significant. A cutoff of 97.5 was used, rather than 95, as clusters from two separate frequency ranges were statistically evaluated (3-13 Hz and 13-90 Hz).

Spiking Analyses

Across rats and sessions, we recorded 114, 459, 437, and 121 well isolated neurons from DG, CA3, CA1, and subiculum, respectively. Putative interneurons were distinguished from these principal cells based on spike-waveforms, autocorrelograms, and firing rates greater than 4 Hz, a cutoff based on both firing rate distributions from the current data and prior reports (e.g., Anderson & O'Mara, 2003; Mizuseki et al., 2012; Ranck, 1973; Skaggs et al., 1996). Principal cell counts were 104, 448, 424, and 59 from DG, CA3, CA1, and subiculum. For comparisons of firing rates across conditions, units were excluded from consideration if they did not emit at least 50 spikes across all conditions. Significant phase modulation of spiking was said to be present for a given neuron if a Rayleigh's Z-Test for circular non-uniformity returned a p-value of less than 0.05. To evaluate whether or not the percent of neurons significantly modulated by phase differed from the percent expected by chance, the actual percent of significantly modulated neurons was compared to the percentages attained from 1,000 shuffles, where, in each of the shuffles, the number of neurons and action potentials was held constant, but spike phase was randomly drawn from a uniform circular distribution.

When assessing spike-phase relationships with nonstationary rhythms (e.g., beta, slow gamma, fast gamma), only spikes occurring when these oscillations are prominent can be considered, as failure to pre-select periods of strong oscillatory activity can lead to spurious detection of spike-phase relationships (Colgin et al., 2009). Thus, when assessing spike-phase relationships to frequency ranges above theta, which is consistently strong throughout the rat hippocampus, we filtered each LFP in the frequency range of interest, then extracted an amplitude envelope for the LFP via a Hilbert transform and detected periods of time in which beta and gamma rhythms were strong for further consideration. We defined oscillatory events as time points in which the amplitude envelope surpassed an edge threshold of at least 1 standard deviation above average and a peak of at least 1.5 standard

deviations above average. Oscillatory events were required to be at least three cycle lengths long, with the cycle length defined by the average frequency for that range. For example, when looking for events in the slow gamma range (30-55 Hz), detected events were required to last at least 70.587 ms in duration, or three full cycles of a 42.5 Hz rhythm, the average frequency of a slow gamma oscillation. Events occurring within 3 average cycle lengths of one another were considered to be the same event.

Spike-phase alignment to the hippocampal theta rhythm by behavioral state (Figure S5) was assessed in relation to theta recorded from the pyramidal layer of CA1, rather than in relation to each subregion's local theta oscillation. The theta oscillation is largely coherent throughout the hippocampus but most readily visible in CA1. Likewise, this procedure allowed for more direct comparisons of spike-phase relationships across subregions. As theta in CA1 is known to exhibit an asymmetric saw-toothed shape rather than a sinusoidal rhythm, we followed the protocol established by Belluscio et al. (2012) when defining the borders between phase components (e.g., peak, falling, trough, rising). In brief, phase centers, established as the peak, trough, and zero crossings of the LFP time series, are first found for a narrowly filtered theta band (6 -12 Hz). The LFP is then re-filtered in a broader band (3 - 20 Hz) and phase centers established from the narrow band are re-defined to be the closest peaks, troughs, and zero-crossings detected in the broader band.

Histology

After experiments were completed, a 20–40 μA current was passed through each recording tetrode for 20-40 s while rats were under anesthesia immediately prior to euthanizing the rat, with the resulting brain lesions serving as confirmation of tetrode position. Transcardial perfusions were performed with 0.9% saline followed by 4% formalin. Brains were extracted and allowed to sit for several days in 4% formalin solution. Brains were moved to a 40% sucrose solution for approximately 72 hours, until brains sank to the bottom of the container, at which point brains were sliced into approximately 70 μm coronal slices and mounted on glass microscope slides. Brains were left for several days to dry in an 37° C oven, then Nissl stained with a cresyl violet solution.

Supplemental References

Anderson, M. I., & O'Mara, S. M. (2003). Analysis of recordings of single-unit firing and population activity in the dorsal subiculum of unrestrained, freely moving rats. *Journal of Neurophysiology, 90*, 655-665.

Belluscio, M. A., Mizuseki, K., Schmidt, R., Kempter, R., & Buzsáki, G. (2012). Cross-frequency phase–phase coupling between theta and gamma oscillations in the hippocampus. *J. Neurosci., 32*, 423-435.

Bragin, A. N. A. T. O. L., Jando, G., Nadasdy, Z., Van Landeghem, M., & Buzsáki, G. (1995). Dentate EEG spikes and associated interneuronal population bursts in the hippocampal hilar region of the rat. *Journal of Neurophysiology, 73*, 1691-1705.

Buzsáki, G. (1986). Hippocampal sharp waves: their origin and significance. *Brain research, 398*, 242-252.

Delorme, A. & Makeig, S. (2004). EEGLAB: An open source toolbox for analysis of single-trial EEG dynamics. *J. Neurosci. Methods*, *134*, 9-21.

Delorme, A., Mullen, T., Kothe, C., Acar, Z.A., Bigdely-Shamlo, N., Vankov, A., & Makeig, S. (2011). EEGLAB, SIFT, NFT, BCILAB, and ERICA: New tools for advanced EEG processing. *Computational Intelligence and Neuroscience*, Article ID 130714.

Ding, M., Bressler, S. L., Yang, W., & Liang, H. (2000). Short-window spectral analysis of cortical event-related potentials by adaptive multivariate autoregressive modeling: data preprocessing, model validation, and variability assessment. *Biol. Cybern. 83*, 35-45.

Gaarskjaer, F. (1986). The organization and development of the hippocampal mossy fiber system. *Brain Res. Rev., 11*, 335-357.

Kaminski, M. J., & Blinowska, K. J. (1991). A new method of the description of the information flow in the brain structures. *Biol. Cybern., 65*, 203-210.

Maris, E., & Oostenveld, R. (2007). Nonparametric statistical testing of EEG-and MEG-data. *J. Neurosci.* Methods, *164*, 177-190.

Maris, E., Schoffelen, J-M., & Fries, P. (2007). Nonparametric statistical testing of coherence differences. *J. Neurosci. Methods, 163*, 161-175.

Mitra, P. P., & Pesaran, B. (1999). Analysis of dynamic brain imaging data. *Biophysical Journal, 76*(2), 691-708.

Mullen, T.R. (2014). The dynamic brain: Modeling neural dynamics and interactions from human electrophysiological recordings (Doctoral dissertation). Available from Dissertations & Theses at University of California; ProQuest Dissertations and Theses A&I. (UMI No. 1619637939)

Ranck, J. B. (1973). Studies on single neurons in dorsal hippocampal formation and septum in unrestrained rats: Part I. Behavioral correlates and firing repertoires. *Exp. Neurol. 41*, 462-531.

Skaggs, W. E., & McNaughton, B. L. (1996). Theta phase precession in hippocampal. *Hippocampus*, *6*, 149-172.

Swanson, L. W., Wyss, J. M., & Cowan, W. M. (1978). An autoradiographic study of the organization of intrahippocampal association pathways in the rat. *J. Comp. Neurol*., *181*, 681-715.

Witter, M. P., & Amaral, D. G. (2004). The hippocampal region. *The Rat Brain (Paxinos G, ed)*, 637-703.